1 The *Plasmodium* NOT1-G Paralogue Acts as an Essential Nexus for Sexual Stage Maturation and Parasite Transmission

2

3 Kevin J. Hart[1], B. Joanne Power[1,^], Kelly T. Rios[1,^], Aswathy Sebastian[2], and Scott E. Lindner[1,#]

4

5 1. Department of Biochemistry and Molecular Biology, The Huck Center for Malaria Research, Pennsylvania State
6 University, University Park, PA 16802
7 2. Huck Institutes of the Life Sciences, Pennsylvania State University, University Park, PA 16802

8 ^. Equal Contributions

9 #. Corresponding Author. Scott E. Lindner (Scott.Lindner@psu.edu, ORCID: 0000-0003-1799-3726)

10

11 Keywords: NOT1, *Plasmodium*, Gametocytogenesis, Zygote, Malaria Transmission

12

Abstract:

Productive transmission of malaria parasites hinges upon the execution of key transcriptional and post-transcriptional regulatory events. While much is now known about how specific transcription factors activate or repress sexual commitment programs, far less is known about the production of a preferred mRNA homeostasis following commitment and through the host-to-vector transmission event. Here we show that *Plasmodium* parasites have taken the unique approach to duplicate the NOT1 scaffold protein of the CAF1/CCR4/Not complex in order to dedicate one paralogue for essential transmission functions. Moreover, this NOT1-G paralogue is central to the sex-specific functions previously associated with its interacting partners, as deletion of *not1-g* in *Plasmodium yoelii* leads to a comparable or complete arrest phenotype for both male and female parasites. We show that, consistent with its role in other eukaryotes, PyNOT1-G localizes to cytosolic puncta throughout much of the *Plasmodium* life cycle. PyNOT1-G is essential to both the complete maturation of male gametes and to the continued development of the fertilized zygote originating from female parasites. Comparative transcriptomics of wild-type and *pynot1-g*$^{-}$ parasites shows that loss of PyNOT1-G leads to transcript dysregulation preceding and during gametocytogenesis, and shows that PyNOT1-G acts to preserve mRNAs that are critical to sexual and early mosquito stage development. Finally, we demonstrate that the tristetraprolin-binding domain, which acts as the typical organization platform for RNA decay (TTP) and RNA preservation (ELAV/HuR) factors is dispensable for PyNOT1-G's essential blood stage functions but impacts host-to-vector transmission. Together, we conclude that *Plasmodium* has created and adapted a NOT1-G paralogue to fulfill the complex transmission requirements of both male and female parasites.

33 **Introduction:**

34 Malaria is still one of the great global health problems of the world today, with nearly two million new reported
35 infections and 400,000 fatalities occurring annually [1]. Transmission of the *Plasmodium* parasites that cause malaria
36 occurs through the bite of a female anopheline mosquito, which transmit liver-infectious sporozoites to initiate a new
37 infection of a mammalian host. Completion of the clinically silent liver stage of development results in the release of
38 membrane-enclosed bundles called merosomes into the blood stream, which are filled with red blood cell-infectious
39 merozoites that can be released upon passage through microcapillaries [2, 3]. Merozoites initiate the asexual blood
40 stage of development, thus initiating a rapid expansion of parasite numbers in the host. However, these asexual blood
41 stage parasites cannot be productively transmitted back to the mosquito. For this, a fraction of blood stage parasites will
42 commit to a sexual developmental program to produce male and female gametocytes, which is dependent upon the
43 ApiAP2-G specific transcription factor [4-6] and is also affected by ApiAP2-G2, which is thought to act as a transcriptional
44 repressor of off-stage transcription [7-9]. In addition, several other protein- and epigenetic-based regulators are central
45 to the commitment to sexual stage development (reviewed in [10, 11]).

46 In contrast, less is known about the effects upon RNA metabolism and translational control during and following the
47 commitment step of *Plasmodium*, which presumably would be regulated by RNA-binding proteins and their binding
48 partners [12]. What is clear is that *Plasmodium* has evolved and adapted common eukaryotic mechanisms for
49 translational repression to promote the efficiency of its transmission, which has been observed in *P. falciparum*, *P.*
50 *berghei*, *P. yoelii*, and *P. vivax* (reviewed in [13]). Among the proteins implicated in *Plasmodium's* translational control of
51 specific mRNAs in female gametocytes are: DOZI (orthologue of a mRNA-decapping activator human DDX6/yeast Dhh1),
52 CITH (orthologue of Lsm14A), PUF-family proteins (PUF1, PUF2), and ALBA-family proteins (ALBA1-4) [14-20]. In
53 addition, the CAF1 and CCR4-1 deadenylase members of the CAF1/CCR4/NOT complex also appear to play an important
54 role in male gametocyte development and in host-to-vector transmission by counterintuitively helping to preserve
55 mRNAs, although the mechanism by which this occurs (e.g. stabilization) remains to be demonstrated [21].

56 In model eukaryotes and human cells, the CAF1/CCR4/NOT complex is best known for its role as the major mRNA
57 deadenylation complex of eukaryotes, but it touches upon many aspects of RNA metabolism from the birth to death of
58 mRNAs, as well as translational repression of specific transcripts (reviewed in [22]). The structure of the complex was
59 solved from *Schizosaccharomyces pombe*, which confirmed the modular nature of this complex with effector proteins
60 being recruited to a central NOT1 scaffold [23]. Together with higher resolution structures of different interaction
61 modules and interacting proteins from several eukaryotes (NOT1 with DDX6, the NOT Module (NOT1-NOT2-NOT5),
62 NOT1 C-terminal domain-NOT4, NOT1 with CAF40, CAF1, CCR4; reviewed in [24]) we have a reasonably good
63 understanding of the overall composition and architecture of this complex. Moreover, the functions of this complex are
64 well known as well. The decay of mRNAs first typically involves the shortening of the poly(A) tail by CAF1/CCR4/NOT

65 and/or Pan2/Pan3 (although Pan2/Pan3 have not been identified in *Apicomplexa*). This is then followed by the removal
66 of the m^7G 5' cap by DCP1/DCP2, which can be activated by a DDX6 protein [25, 26]. Finally, the now unprotected mRNA
67 is degraded by 5' to 3' and 3' to 5' exonucleases.

68 In these processes, NOT1 acts as a central nexus for the overall functions of its complex. Because NOT1 acts as an
69 essential scaffold and yet lacks enzymatic activity of its own, recruitment of the appropriate effector proteins and their
70 regulators is critical for the function of this complex. In addition to the proteins noted above, ELAV-family proteins and
71 tristetraprolin (TTP) are recruited and act as antagonistic, mutually exclusive modulators to functionally toggle the
72 complex's activity between transcript preservation vs. transcript degradation [27]. ELAV-family proteins (which include
73 HuR and CELF proteins) and TTPs (which are C3H1 zinc finger proteins, and include ZFP36, TIS11) are RNA-binding
74 proteins that bind with AU-rich elements in eukaryotes [28]. In addition to its roles in RNA metabolism, recently it was
75 shown that the CAF1/CCR4/NOT complex acts to monitor for low translational efficiency. In this work, NOT5 was found
76 to associate with ribosomes attempting to translate suboptimal codons by binding the ribosomal E-site in its post-
77 translocation state [29]. Those authors proposed that the association of CAF1/CCR4/NOT and Dhh1 (the orthologue of
78 DDX6, DOZI) with these ribosomes prompts co-translational decay of these mRNAs with an abundance of suboptimal
79 codons via deadenylation and decapping. As the localization of Dhh1 and orthologues to cytosolic processing bodies is
80 associated with its activity, it is notable that the association of NOT1 with Dhh1 acts to inhibit the assembly of
81 processing bodies in yeast [30]. Taken together, as NOT1 itself lacks any enzymatic activities, it brings together protein
82 effectors that can degrade or preserve mRNAs and can selectively target mRNAs that are not optimally coded for
83 translation. Due to key differences between *Plasmodium* and other eukaryotes, such as its extreme AU-rich
84 transcriptome, it is not certain if the same activities are used in the same ways in *Plasmodium* parasites.

85 Previous work that aimed to determine whether *Plasmodium* uses the CAF1/CCR4/NOT complex similarly was first
86 focused on the *P. falciparum* CAF1 deadenylase, which was identified through the *piggyBac* transposon screen [31].
87 While initially thought to be dispensable, further experiments demonstrated that only the conserved N-terminal CAF
88 domain was essential and remained expressed with the *piggyBac* insertion [21]. We have recently shown that both the
89 specialty CCR4-1 deadenylase and the generalist CAF1 deadenylase are critical for RNA metabolism in gametocytes and
90 affect the synchronicity of male gametocytogenesis and transmission to mosquitoes [21]. In this work, we
91 experimentally identified that the CCR4-1 deadenylase interacts with canonical members of the CAF1/CCR4/NOT
92 complex (NOT2, NOT4, NOT5, CAF40), including both deadenylases (CCR4-1, CAF1), as well as the *Plasmodium*
93 orthologue of DDX6 (DOZI), CITH, an ELAV-family protein (CELF2/Bruno/HoBo), and more. Moreover, we also identified
94 ribosomal proteins, suggesting that a physical link between CAF1/CCR4/NOT via NOT5 could be present in *Plasmodium*
95 as has been seen for model eukaryotes [29]. Through label-free quantification, we also identified a highly abundant, but
96 uncharacterized protein annotated simply as "NOT Family Protein."

97 Here we demonstrate that in contrast to other sequenced eukaryotes, *Plasmodium* and two related parasites have
98 duplicated the *not1* gene and has dedicated one of the paralogues for essential transmission-related functions. We have
99 reannotated these paralogues as NOT1 and NOT1-G according to their phenotypes and functions. We show that NOT1-G
100 is responsible first for a slight dampening of the production of gametocytes, and yet then promotes the maturation and
101 fertility of those gametocytes that do commit. PyNOT1-G affects both sexes, as it is essential for the production of male
102 gametes and the continued development of fertilized female gametes in early mosquito stage development. Because
103 the CAF1/CCR4/NOT complex associates with members of the DOZI/CITH/ALBA complex in *P. yoelii*, these phenotypes
104 indicate that PyNOT1-G is a central and essential organizer of gametocyte development.

105

106 **Results:**

107 **Parasites of the Aconoidasida Class have Duplicated the *not1* Gene**

108 Control of mRNA metabolism is a central feature of eukaryotic gene regulation. The CAF1/CCR4/NOT complex plays
109 many central roles in these processes from the birth to the death of mRNAs, with its best appreciated role being in the
110 decay of the poly(A) tail of mRNAs. Previously, we and others have demonstrated the importance of the CAF1 and CCR4-
111 1 deadenylases of this complex to the sexual development of both rodent-infectious and human-infectious malaria
112 parasites (*Plasmodium yoelii* and *Plasmodium falciparum*, respectively) [21, 31]. In our previous efforts to experimentally
113 determine the composition of the CAF1/CCR4/NOT complex in *Plasmodium* through mass spectrometry-based
114 proteomics, we identified a protein annotated only as "NOT Family Protein" (PY17X_1027900) that was found to be
115 associated with CCR4-1 [21] . Bioinformatic analyses using PlasmoDB and BLASTp identified that the protein encoded by
116 PY17X_1027900 mostly closely matched eukaryotic NOT1 proteins, but lacked a bioinformatically predictable
117 tristetraprolin (TTP)-binding domain that is present in the gene currently annotated as NOT1 (PY17X_0945600) (Figure 1)
118 [32, 33]. Because no other sequenced eukaryotes to date have an annotated duplication of *not1*, we used bioinformatic
119 sequence comparisons to explore this further. We concluded that these two *not1* genes were paralogues due to the high
120 degree of sequence conservation in specific domains at both the DNA and protein levels (DNA: CAF1-binding domain
121 72% identity, NOT4-binding domain 66% identity; Protein: CAF1-binding domain 41% identical/63% positive, CAF40-
122 binding domain 33%/57%, NOT4-binding domain 48%/62%, NOT1 domain 50%/73%). Moreover, these genes are highly
123 conserved, syntenic, and only present across *Plasmodium* species and two other species of the Aconoidasida class
124 (Genera: *Theileria*, *Babesia*), but not in other apicomplexans, model eukaryotes, or humans. Together, this provides
125 evidence that these are paralogs of NOT1 that arose from a gene duplication in the common evolutionary ancestor [34].
126 As these parasites share some common traits for their transmission strategies between mammals and insects that are

127 not shared with other apicomplexans, we hypothesized that this NOT1 paralogue may have evolved for specialized
128 functions during parasite transmission.

129

130 ***Plasmodium's* NOT1 Paralogues Localize to Cytosolic Puncta**

131 Due to the central roles that the CAF1/CCR4/NOT complex plays in RNA metabolism in eukaryotes, this complex is
132 typically found in the nucleus and/or in cytosolic puncta associated with complexes in the spectrum between stress
133 granules and processing bodies (P-bodies) [22, 35]. Representative members of this complex (CAF1, CCR4-1) in
134 *Plasmodium* also have this expression and localization profile and are found predominantly in cytosolic puncta and
135 associate with proteins that are commonly associated with these granules [21]. To determine if the two paralogues of
136 NOT1 are used at different points in the *Plasmodium* life cycle, we used conventional reverse genetics approaches to
137 append a C-terminal GFP tag to each NOT1 paralogue in *P. yoelii* (Supplemental Figure 1) and assessed their expression
138 and localization (Figure 2, Supplemental Figure 2). Both NOT1 paralogues were expressed and localized at the same
139 times in the life cycle, and both are predominantly found as cytosolic puncta as was seen for other members of the
140 CAF1/CCR4/NOT complex in *Plasmodium yoelii*. Of note, the NOT1 paralogues were expressed in both asexual and
141 sexual blood stage parasites with a non-uniform, cytosolic distribution with some puncta visible. Both paralogous
142 proteins were expressed in mosquito stage parasites, with localization shifting from a cytosolic diffuse pattern in
143 oocysts, to a more nucleus-proximal pattern in oocyst sporozoites, and finally to a more apical pattern in salivary gland
144 sporozoites. No expression of either protein was observed in mid- or late-liver stage parasites. Together, these
145 expression and staining patterns match what is commonly seen for members of the CAF1/CCR4/NOT complex in other
146 eukaryotes, as well as what we observed previously in *P. yoelii* with two other members of this complex: CAF1 and CCR4-
147 1 [21]. Coupled with proteomic data showing their association with CCR4-1, this strongly indicates that these NOT1
148 paralogues are resident members of the CAF1/CCR4/NOT complex in *Plasmodium yoelii*.

149

150 **PyNOT1 (PY17X_1027900) is Critical for Asexual Blood Stage Growth in *P. yoelii***

151 NOT1 is essential and acts as a central scaffold to nucleate several RNA-centric functions in eukaryotes [22]. The
152 CAF1/CCR4/NOT complex is most well-known for its role in mRNA deadenylation, but also contributes to transcriptional
153 initiation and elongation, translational repression, mRNA export, and nucleus-based quality control activities. To
154 determine if either *Plasmodium* NOT1 paralogue bore a greater functional semblance to canonical NOT1 proteins in
155 eukaryotes or had dedicated functions in *Plasmodium*, we used conventional reverse genetics approaches to delete the
156 coding sequence of each paralogue, which was confirmed by genotyping PCR (Supplemental Figure 3).

157 In agreement with the critical/essential role of NOT1 to eukaryotic RNA metabolism, our attempts to delete
158 *py17x_1027900* were largely unsuccessful. However, in one of two technical duplicates of six independent transfection
159 attempts, we were able to obtain a 100% transgenic population with an extremely slow growth phenotype. It was only
160 possible to produce this parasite line because the population was entirely transgenic, as the presence of even a small
161 number of wild-type parasites with *de novo* resistance to pyrimethamine would likely have rapidly outgrown these
162 transgenic parasites in the mouse. These data align with results from both PlasmoGEM (*P. berghei*) and *piggyBac* (*P.*
163 *falciparum*) genetic screens that noted the importance of this gene to asexual blood stage growth [36-38]. Due to the
164 severe asexual blood stage defect, which closely aligned with observations of NOT1-related phenotypes in other
165 eukaryotes, we propose that this "NOT Family Protein" is truly the NOT1 protein of *Plasmodium* parasites. Finally, it is
166 notable that in contrast to other eukaryotes, PyNOT1 can be deleted and indicates that it is not strictly essential.

167 **PyNOT1-G (PY17X_0945600) Dampens Sexual Stage Commitment but is Essential for Sexual Maturation**

168 In stark contrast, the paralogous gene currently annotated as NOT1 (*py17x_0945600*) was readily deleted and multiple
169 independent clones were obtained by limited dilution cloning (Supplemental Figure 3B). This was unexpected given the
170 essential role of NOT1 in all other eukaryotes and lends further credence to the assignment of the first paralogue
171 described above as the true NOT1 protein of *Plasmodium* parasites. The ability to disrupt this gene was corroborated by
172 the *piggyBac* screen in *P. falciparum*, which identified that transposon insertions in this gene could still produce viable
173 parasites [36].

174 In order to determine if *py17x_0945600* plays a specialized role in *Plasmodium* growth, development, or transmission,
175 mice were infected with 10,000 Py17XNL wild-type parasites or clonal *py17x_0945600*-null parasites and the progression
176 of the asexual blood stage infection was monitored by daily Giemsa-stained thin blood smears in technical and biological
177 triplicate. No significant asexual blood stage growth defects were observed for *py17x_0945600*-null parasites until late
178 in the blood stage infection (day 10). At this point, there was a small, but statistically significant decrease in peak
179 parasitemia with a concomitant earlier time to parasite clearance (Figure 3A).

180 One explanation for this defect could be due to an overcommitment to gametocytogenesis in the absence of this gene
181 product, as committed male and female parasites are differentiated cells and cannot contribute to increasing the total
182 parasitemia further. Moreover, this asexual blood stage growth defect became pronounced approximately when
183 gametocyte numbers begin to be abundant in the *P. yoelii* 17XNL strain (~1% parasitemia). To assess this, we compared
184 the total gametocytemia of Py17XNL WT-GFP parasites and *py17x_0945600*-null parasites following treatment with a 2-
185 day course of sulfadiazine to selectively kill asexual blood stage parasites and to leave gametocytes in circulation. By a
186 flow cytometric assay to count GFP-expressing parasites, we observed a slight increase in gametocytogenesis (27-35%
187 increase, unpaired t test with Welch correction, $p = 0.04$) in *py17x_0945600*-null parasites compared to wild-type

188 parasites (Figure 3B, Supplemental File 2). The increase in gametocytemia paired with the decrease in asexual blood
189 stage parasitemia, may indicate that PY17X_0945600's role in wild-type parasites is to slightly dampen commitment to
190 gametocytogenesis . To assess this effect upon gametocytes further, the same mice that were used to assess the asexual
191 blood stage growth kinetics were also monitored for the presence of male gametes through observation of exflagellation
192 centers ("centers of movement") (Figure 3C). We observed no exflagellating male gametes throughout the entire course
193 of blood stage infection, indicating that PY17X_0945600 is essential for either gametocyte maturation and/or
194 gametogenesis. Taken together, we have reannotated PY17X_0945600 as PyNOT1-G due to its dual and opposed
195 functions to perhaps dampen gametocyte commitment and yet act in an essential manner to drive male gametocyte
196 maturation.

197 **PyNOT1-G is Essential to Zygote Development**

198 While these data indicate the PyNOT1-G is essential for the complete maturation of male parasites, these experiments
199 did not directly study the impact of PyNOT1-G on female gametocytes or upon host-to-vector transmission. To address
200 these questions, we conducted a genetic cross experiment with Py17XNL wild-type parasites that do not express a
201 fluorescent protein and *pynot1-g*$^-$ parasites that express GFPmut2 from a constitutive promoter integrated in the
202 *pynot1-g* locus. If either male or female *pynot1-g*$^-$ parasites were viable for transmission either by self-fertilization or by
203 crossing with wild-type parasites, GFP-expressing oocysts would be evident in the mosquito (Figure 4A). In contrast, if
204 only wild-type male and female parasites were fertile, only non-fluorescent oocysts would be observed. In three
205 independent transmission experiments, donor mice infected with either Py17XNL wild-type parasites or *pynot1-g*$^-$
206 parasites were used to produce parasites for IV transfer of 1) 10,000 wild-type parasites, 2) 5000 wild-type parasites +
207 5000 *pynot1-g*$^-$ parasites, or 10,000 *pynot1-g*$^-$ parasites into experimental mice. Parasitemia increased to 1% with the
208 same timing in all mice and exflagellating male gametes were observed in mice infected with wild-type parasites or a
209 combination of wild-type and *pynot1-g*$^-$ parasites, but were not seen with infections with *pynot1-g*$^-$ parasites. Mice were
210 anesthetized and mosquitoes were allowed to blood feed for one period of 15 minutes. Seven days post-blood meal,
211 midguts were removed and oocysts were counted and scored by DIC and fluorescence microscopy. No oocysts were
212 detected in mosquitoes that fed upon mice infected with *pynot1-g*$^-$ parasites, which is consistent with the absence of
213 exflagellating male *pynot1-g*$^-$ gametes (Figure 3C). However, in mosquitoes that fed upon wild-type parasites or a
214 mixture of wild-type and *pynot1-g*$^-$ parasites, only non-fluorescent oocysts were detected thus indicating that both male
215 and female *pynot1-g*$^-$ parasites are unable to productively transmit to mosquitoes. Additionally, the effect upon both
216 sexes of *pynot1-g*$^-$ parasites was further corroborated by the presence of approximately half of the number of oocysts in
217 mosquitoes that fed upon the mixture of wild-type and *pynot1-g*$^-$ parasites as compared to those that fed upon only
218 wild-type parasites. This indicates that PyNOT1-G is an essential driver of maturation for both male and female
219 *Plasmodium* parasites.

220 As these defects in *pynot1-g*$^-$ parasites parasite transmission could result from a block in early mosquito stage
221 development of female parasites, we used an *in vitro* genetic cross approach to determine if either sex of *pynot1-g*$^-$
222 parasites could produce zygotes or ookinetes. As controls, we used PyWT-mScarlet (Py1115) and PyWT-GFP (Py489)
223 transgenic lines. As anticipated, we found that wild-type parasites could readily self-cross (GFP+/mScarlet-, GFP-
224 /mScarlet+) and cross (GFP+/mScarlet+) to yield zygotes, retorts and ookinetes (Figure 4B). In contrast, experiments that
225 crossed PyWT-mScarlet with GFP-expressing *pynot1-g*$^-$ parasites could not yield *pynot1-g*$^-$ self-crossed zygotes but could
226 yield crossed (GFP+/mScarlet+) zygotes that failed to develop further (Figure 4B). This female-specific phenotype
227 matches that seen previously for *pbdozi*$^-$ and *pbcith*$^-$ parasites and indicates that PyNOT1-G may play an important role
228 in preparing the female gametocyte for further development [19, 20].

229

230 **Extensive Transcriptomic Dysregulation in *pynot1-g*$^-$ Schizonts and Gametocytes**

231 As the CAF1/CCR4/NOT complex can contribute toward both mRNA preservation and mRNA decay activities in
232 *Plasmodium* and other eukaryotes [21, 22], we used total comparative RNA-seq (WT vs *pynot1-g*$^-$ parasites) to assess
233 differences in transcript abundances in both mixed male and female gametocyte populations and asexual blood stage
234 schizonts depleted of rings, trophozoites, and gametocytes through a subtractive magnetic approach. A variance
235 stabilizing transformation (vsf) of the sample raw counts was used to generate a heatmap and a PCA plot of these data,
236 both of which show good within-group clustering and separation of different sample types (Figure 5AB). MA plots and
237 Volcano plots of gametocytes (Figure 5C, 5E) and schizonts (Figure 5D, 5F) show differential expression of specific
238 transcripts in both stages that is dependent upon PyNOT1-G.

239 First, we further examined the effect of PyNOT1-G in gametocytogenesis through these comparative RNA-seq data of
240 Py17XNL wild-type and *pynot1-g*$^-$ gametocytes (Figure 5C, 5E, Supplemental Table 1). In addition to the use of DEseq2,
241 we have also imposed a Transcript Integrity Number (TIN) metric to help identify and remove reads due to run-in
242 transcription [39, 40]. We observed that *pynot1-g*$^-$ gametocytes had lower abundances of 427 transcripts (threshold of ≤
243 $\log_2$ -2.5), including a substantial number of gametocyte-enriched (*p25*, *p28*, three *apiap2* transcripts, *imc*-related
244 transcripts, *ccp* family transcripts, *cpw-wpc* family transcripts, *migs*, and *actin II*) and early mosquito stage (*ctrp*, *warp*,
245 *psop* family transcripts, and *perforins*) transcripts [4, 41]. Notably, the transcript abundance of the NOT1 paralogue
246 (*pynot1*) was not affected, whereas *pyapiap2-g*, the master regulator of commitment to gametocytogenesis, was down
247 $\log_2$ -1.2 (2.3-fold reduction) in *pynot1-g*$^-$ parasites. Enriched GO terms include cellular component terms related to the
248 cytoskeleton, microtubules/actin, and molecular function terms related to binding to the cytoskeleton (Supplemental
249 Table 1). In contrast, few transcripts had increases in abundance (threshold of ≥ $\log_2$ 2.5), but those that were more
250 abundant are from off-stage genes related to invasive stages and/or sporozoites. Further expansion of the threshold (≥

251 $\log_2$ 2.0) then included many more off-stage, apical organelle gene products (MSP family, RON family, RhopH family, RAP
252 family, SERA family, MAEBL, TREP).

253 This transcriptional dysregulation is catastrophic for male gametocytes, as they are unable to complete gametogenesis.
254 However, despite this substantial dysregulation of transcript abundances, it is remarkable that female gametocytes are
255 still permissive to form female gametes, which can be fertilized by competent wild-type male gametes. However,
256 because development arrest occurs at the zygote stage, this indicates that the RNA homeostasis promoted by the
257 PyNOT1-G complex is essential for further development, as was seen for studies of PbDOZI and PbCITH [19, 20]. In
258 agreement with this, we compared differentially expressed transcripts from *pynot1-g*$^-$ and *pbdozi*$^-$ and/or *pbcith*$^-$
259 parasites, and found that 98 of the 115 transcripts that are ≤ $\log_2$ -1 in *pbdozi*$^-$ and/or *pbcith*$^-$ are also reduced in
260 abundance ≤ $\log_2$ -2.5 in *pynot1-g*$^-$ parasites. By matching the reporting thresholds to ≤ $\log_2$ -1, nearly all (105/115) of the
261 transcripts that are lower in abundance in *pbdozi*$^-$ and/or *pbcith*$^-$ parasites are also in lower abundance in *pynot1-g*$^-$
262 parasites. This highly similar effect may be attributable to these proteins working in concert, as DOZI and CITH are
263 known to interact with the CAF1/CCR4/NOT complex in *Plasmodium* and other eukaryotes [21, 22]. Additionally, many
264 of the same transcripts that are similarly dysregulated in the *pyalba4*$^-$ line are also dysregulated in *pynot1-g*$^-$ parasites
265 (265 of 438 transcripts are ≤ $\log_2$ -1 in both lines) [14]. Finally, 81 transcripts are similarly dysregulated across all four
266 transgenic parasite lines (*pbdozi*$^-$, p*bcith*$^-$*, pynot1-g*$^-$*, pyalba4*$^-$), and include *p25*, *lccl* family, IMC-related, *ap2-o*, *warp*,
267 and *psop* family gene products (Supplemental Table 2). These results also have extensive overlap with PbDOZI-
268 associated transcripts identified by RIP-chip (409 of 1046 transcripts) [16].

269 However, as we also determined that PyNOT1-G has an impact on the peak and clearance of asexual blood stage
270 growth, we also assessed changes in transcript abundance in asexual blood stage schizonts that can already be in the
271 process of commitment. As blood stage infections of *P. berghei* and *P. yoelii* often contain a significant number of
272 gametocytes (10% of total parasites), we developed a magnet-based subtractive separation approach to remove
273 trophozoites, schizonts, and gametocytes from the sample through four serial passes over magnetized columns. Flow
274 cytometric analyses demonstrated that gametocytes consisted of <1% of the remaining parasites, and that additional
275 passes through the magnetized columns provided no additional enrichment (data not shown). The remaining ring stage
276 parasites were cultured *ex vivo* until they reached a mature schizont stage based upon Giemsa staining, and then were
277 subjected to total comparative RNA-seq.

278 Here we observed similar trends in the differential abundance of mRNAs that could be directly or indirectly preserved by
279 PyNOT1-G and its complex in schizonts (Figure 5D, 5F, Supplemental Table 3). Those 293 mRNAs that are less abundant
280 in *pynot1-g*$^-$ schizonts include many classic and recently defined early gametocyte transcripts [4, 41]. These include many
281 mRNAs that are translationally repressed in *P. berghei* and/or *P. falciparum*, such as *p25* and *p28* (49.5-fold and 74.6-
282 fold reductions) as well as several members of the *psop*, *lccl*, and *ccp/lap* gene families. Moreover, other transcripts that

283 were also dysregulated in gametocytes were similarly dysregulated in schizonts, including *warp*, *hsp20*, *migs*, *soap*,
284 *p230p*, *p48/45*, *gest*, *gamete egress protein* (*gep*), *male development protein 1* (*mdv1*), *plasmepsin vIII*, and *actin ii*.
285 Notably, *pyapiap2-g* is also down $\log_2$ -2.3 (~5-fold) in schizonts. Statistically significant GO terms related to these
286 transcripts, and to processes downstream of the schizont stage, include cellular component terms related to the
287 crystalloid, cytoskeleton, microtubules, and dynein, molecular function terms related to motor activity, and biological
288 process terms related to meiosis, microtubules, and movement. Together this indicates that the specific transcripts that
289 are regulated by PyNOT1-G in gametocytes are also affected by it prior to gametocytogenesis, suggesting that the
290 setting of a preferred RNA homeostasis for host-to-vector transmission may occur earlier than anticipated. It remains to
291 be determined if PyNOT1-G and its complex acts to stabilize mRNAs, or if it acts in some other way to preserve the
292 abundance of specific mRNAs. Importantly, these multifaceted roles of PyNOT1-G in RNA metabolism match and exceed
293 the roles seen with CCR4-1 (one of the deadenylases of this complex) and the DOZI/CITH/ALBA4 that can associate with
294 it [14, 19-21].

295

296 **The Tristetraprolin-Binding Domain of PyNOT1-G is Dispensable for its Essential Roles in Blood Stage Parasites, but is**
297 **Important for Transmission**

298 The diverse functions of the CAF1/CCR4/NOT complex rely upon the associations of diverse regulators with the NOT1
299 scaffold to direct its activities to specific mRNAs. One such pair of antagonizing RNA-binding regulators, ELAVs
300 (embryonic lethal abnormal vision, Hu family of proteins (HuR)) and tristetraprolin (TTP, C3H1 RNA-binding Zinc Finger
301 Proteins), bind to the same TTP-binding domain on NOT1 proteins and functionally toggle this complex between
302 transcript preservation and transcript degradation respectively [28]. While ELAV-like/HuR proteins can be
303 bioinformatically predicted and have been found associated with the CAF1/CCR4/NOT and DOZI/CITH/ALBA regulatory
304 complexes (CELF1, CELF2/Bruno/HoBo), a *Plasmodium* TTP orthologue cannot similarly be predicted with confidence
305 [14, 21, 42]. The only bioinformatically discernable difference between the two NOT1 paralogues was the presence of a
306 conserved tristetraprolin (TTP)-binding domain (AA7-164) on NOT1-G, which is strongly conserved across *Plasmodium*
307 species (e.g. 100% identical in *P. berghei* ANKA, 73% identical/88% similar in *P. falciparum* NF54, 80% identical/92%
308 similar in *P. vivax*), but that cannot be detected on PyNOT1 or its orthologues in other *Plasmodium* species (Figure 1).

309 To this end, we used two complementary approaches to examine the importance of this putative TTP-binding domain to
310 the function of PyNOT1-G. First, we created a transgenic parasite line using the strong, constitutive *pbeef1a* promoter to
311 overexpress the TTP-binding domain (AA1-199) of PyNOT1-G fused to GFPmut2 (TTPbd::GFP) from a safe harbor locus
312 (*pyp230p*) (Supplemental Figure 4A). Expression boundaries for this protein variant were chosen based upon the use of
313 domain predictions along with the presence of an enriched region of asparagine residues in *P. yoelii* that is even more

314 pronounced in *P. falciparum*, as these regions are often found between functional domains in *Plasmodium* proteins. We
315 hypothesized that overexpression of TTPbd::GFP would act dominant negatively by binding and sequestering proteins
316 that need to interact with PyNOT1-G to be effective. Expression of TTPbd::GFP was observed by western blotting of the
317 immunoprecipitated protein vs control WT-GFP parasites (Supplemental Figure 4B). Despite this, we did not observe any
318 statistically significant defects in asexual blood stage growth or the ability of these parasites to produce exflagellating
319 male gametes (Figure 6AB). Moreover, in stark contrast to *pynot1-g*$^{-}$ parasites, the TTPbd::GFP-overexpressing parasites
320 were competent for transmission to mosquitoes (Supplemental Table 4). This indicates that overexpression of PyNOT1-
321 G's TTP-binding domain does not act dominant negatively, perhaps because it could be insufficient to sponge away the
322 relevant factors and/or because this domain and its interacting partners may not be essential to PyNOT1-G's functions in
323 gametocytes.

324 Second, we created a transgenic parasite lacking the TTP-binding domain of PyNOT1-G by replacing those sequences
325 with GFPmut2 (ΔTTPbd). Clonal lines were isolated and compared to Py17XNL WT-GFP parasites (Supplemental Figure
326 4C). As with the TTPbd::GFP overexpression line, no statistically significant defect in asexual blood stage growth or in the
327 numbers of exflagellating male gametes was detected (Figure 6CD). However, statistically significant effects upon the
328 prevalence of mosquito infection were observed (multiple unpaired t-test, no assumptions of standard deviation, $p =$
329 0.006763 (WT vs Clone 1, $p = 0.030700$ (WT vs Clone 2)) but not for the number of oocysts per infected mosquito (Table
330 1). This indicates that the TTP-binding domain of PyNOT1-G, and by interference proteins that require it to interact with
331 PyNOT1-G, are ultimately dispensable for PyNOT1-G's functions in male gametocytogenesis and/or gametogenesis and
332 female parasite development beyond the zygote stage, but yet it appears to play a significant role in host-to-vector
333 transmission. In contrast, the remaining portions of PyNOT1-G are essential for these functions and thus may provide
334 additional interaction points for these regulatory proteins.

335

336 **Discussion:**

337 Here we describe the unique duplication and adaptation of a NOT1 paralogue for the transmission requirements of
338 malaria parasites. Due to the high degree of DNA identity and amino acid similarity/identity, these genes likely arose due
339 to a duplication event. It is notable that the same domain organization of two NOT1 paralogues is also present in the
340 closely related apicomplexans *Babesia* and *Theileria*, while this duplication is not evident in *Toxoplasma* or other
341 apicomplexans that have evolved other transmission strategies (Figure 1). To our knowledge, this duplication of NOT1 is
342 unique to the Aconoidisida class. This duplication of NOT1 has been noted in preliminary findings in *Plasmodium*
343 *falciparum* asexual blood stage parasites presented in a recent preprint [43]. In that work, the transgenic *P. falciparum*
344 parasites (and presumably the parental parasites used to generate them) could not generate gametocytes and thus

345 those studies were focused on discerning differences in their functions within the asexual blood stage. Here we also
346 observe effects upon asexual blood stage growth, which were extreme when *pynot1* is deleted, but which were more
347 muted when *pynot1-g* is deleted. In contrast, here we show that the major essential roles of PyNOT1-G are in the
348 development of male and female gametocytes/gametes, and the continuing development of the fertilized zygote in
349 early mosquito stage.

350 Consistent with their domain architecture and protein interactions, we found that PyNOT1 and PyNOT1-G localize to
351 cytosolic puncta reminiscent of regulatory mRNP granules that are observed in many eukaryotes including *Plasmodium*.
352 We and others have also observed this localization for CAF1, CCR4-1, ALBA4, DOZI, and CITH, which also interact with
353 one another in specific contexts and life cycle stages [14, 19, 21]. Through extensive reverse genetic attempts, we were
354 only able to isolate a completely transgenic parasite population where *py17x_1027900* (*pynot1*) was deleted, as the
355 presence of any wild-type parasites would likely outcompete it rapidly. We now propose the reannotation of this gene
356 as the canonical NOT1 as it matches the hallmarks of NOT1 from other eukaryotes, including an extremely slow growth
357 phenotype when its gene is deleted [22]. It is interesting that *pynot1* could be deleted at all given its central and
358 essential role in the activities of the CAF1/CCR4/NOT complex in model eukaryotes. This suggests that the organizing
359 functions provided by the PyNOT1 scaffold can presumably be achieved by subcomplexes, or by proteins that can act in
360 a functionally redundant manner, perhaps by PyNOT1-G although this remains to be experimentally determined.

361 Here we have focused on the NOT1 paralogue that does not behave like any other eukaryotic NOT1, which we have
362 termed PyNOT1-G due to its essential roles in *Plasmodium* gametocytes and gametes. The timing of a slight asexual
363 blood stage growth defect in *pynot1-g*$^{-}$ correlates with the typical onset of a wave of commitment to gametocytogenesis
364 and thus may correlate with the 27-35% increase in gametocyte numbers observed (Figure 3B). Furthermore, changes in
365 transcript abundance in asexual blood stage schizonts depleted of gametocytes indicated that several mRNAs relevant to
366 early gametocytogenesis are preserved by PyNOT1-G quite early on, and include transcripts for *male development gene*
367 *1* (*mdv1*), *actin ii*, *p25*, *p28*, *gest*, and several others. The ApiAP2-G specific transcription factor, which acts as a master
368 regulator of commitment to gametocytogenesis was also dysregulated at the transcript level. However, we observed
369 that *pyapiap2-g* mRNA levels were lower in both schizonts and gametocytes, which is discordant with the expectation
370 that fewer gametocytes would form. Instead, we observed that gametocyte levels were slightly elevated (Figure 3B,
371 Figure 5). This would indicate that *pyapiap2-g* mRNA levels alone are not responsible for how extensively parasites
372 commit to sexual development, and that other factors contribute to this as well. Finally, we have intentionally used the
373 general descriptor "preserve" when describing PyNOT1-G's effect upon transcript abundance, as it remains to be
374 demonstrated for any *Plasmodium* protein implicated in translational repression or related complexes that a stabilizing
375 effect is produced, although we hypothesize that this would be the case.

376 Transcriptomics of gametocytes also reflect that males are severely affected and is consistent with their inability to
377 complete gametogenesis to produce exflagellating gametes. Many of the transcripts that are dysregulated in schizonts
378 are also dysregulated in gametocytes and in some cases to an even greater extent. In considering female-enriched
379 transcripts, there is a high overlap in the specific mRNAs that are dysregulated by a deletion of *pynot1-g*, *pyalba4*,
380 *pbdozi*, or *pbcith* (Supplemental Table 2), and a common phenotype in female parasites when *pynot1-g*, *pbdozi*, or
381 *pbcith* is deleted. This indicates that this level of female-enriched transcript dysregulation is permissive to allow
382 gametogenesis and fertilization by a competent male, but it appears to prevent further development of the zygote. This
383 aligns with the classic model of the maternal-to-zygotic transition, where pre-made mRNAs are produced, stored, and
384 translationally repressed/silenced until fertilization occurs [44].

385 Here we find that PyNOT1-G primarily acts to promote male gametocytogenesis and/or gametogenesis as evidenced by
386 the complete absence of male gametes and a transcriptomic profile that reflects severe dysregulation of male-enriched
387 mRNAs (Figure 5). Unsurprisingly, male *pynot1-g*$^{-}$ parasites are also unable to transmit to mosquitoes (Figure 4A).
388 Moreover, the inability of female parasites to produce viable zygotes that can develop into ookinetes *in vitro* (Figure 4B),
389 or oocysts *in vivo* (Figure 4A) matches the phenotypes previously observed for deletions of *pbdozi* and *pbcith*. Together,
390 it is clear that PyNOT1-G acts upon both sexes and matches or exceeds the phenotypes observed previously for the
391 deletion of genes for its key interaction partners.

392 Our previous work demonstrated that both PyNOT1 and PyNOT1-G are capable of binding with the PyCCR4-1
393 deadenylase [21]. As NOT1 acts as a scaffold onto which other factors assemble, it is anticipated that NOT1 and NOT1-G
394 are mutually exclusive members of discrete complexes, although this remains to be formally and robustly demonstrated.
395 What is clear is that canonical CAF1/CCR4/NOT proteins, as well as possible ELAV/HuR and TTP candidates, all associate
396 with this complex. As the functions of NOT1 in other eukaryotes can be toggled based upon the antagonistic association
397 of ELAVs/HuRs or TTPs, our finding that this predicted TTP-binding domain is not important for NOT1-G functions in
398 gametocyte biology is possibly surprising. One explanation for why *Plasmodium* may have evolved away from the use of
399 this toggle in this rare NOT1 paralogue could be due to its extreme AT-rich genome and resulting AU-rich transcriptome.
400 As ELAV/HuR and TTP typically bind with AU-rich elements on target mRNAs, this strategy would not provide much
401 regulatory specificity in *Plasmodium*. Thus, different or additional parameters may be employed to ensure on-target
402 regulation occurs. Consistent with this hypothesis, we identified other zinc finger proteins associated with this complex,
403 including one (PY17X_0417500) with a triple C3H1 ZnF configuration with predicted roles in mRNA decay. It will
404 therefore be interesting to determine if and how these effector proteins associate with PyNOT1-G independently of the
405 TTP-binding domain, and to determine how these proteins can regulate only selected mRNAs given how frequently AU-
406 rich mRNA sequences can be found in *Plasmodium*.

407 In order to synthesize our current understanding of how *Plasmodium* blood stage proteins implicated in translational
408 repression (or with complexes known to be translationally repressive) may interact, we have reanalyzed published
409 datasets to propose a composite network based upon formaldehyde crosslinking IP/MS datasets for PbDOZI::GFP,
410 PbCITH::GFP, and PyALBA4::GFP from gametocytes and PyCCR4-1::GFP from schizonts [14, 19, 21] (Figure 7). We also
411 attempted to provide reciprocal proteomics data using PyNOT1-G as the bait (e.g. immunoprecipitation +/- chemical
412 crosslinking, BioID, TurboID), but because these experiments did not provide additional insights using only highly
413 stringent statistical cutoffs, we have not included them in this model. Moreover, it is notable that the phenotypes for
414 *pynot1-g*$^{-}$ transgenic parasites are identical to those for *pbdozi*$^{-}$ / *pbcith*$^{-}$ (female gametocytes can activate into gametes
415 and be fertilized, but cannot develop further) and more extreme than those for *pyccr4-1*$^{-}$ or the truncation of *pycaf1*
416 (complete arrest vs. partial defects in either male gametocyte development or gametogenesis). Taken together with
417 proteomic evidence, and consistent with the general role of NOT1 in model eukaryotes and humans, we propose that
418 PyNOT1-G has been evolved to act as a central organizing nexus for these regulatory activities for both sexes of
419 parasites, whereas DOZI/CITH and CCR4-1/CAF1 have sex-specific roles. Additionally, preliminary results from a preprint
420 indicate that the *P. falciparum* NOT1 and NOT1-G orthologues are mutually exclusive in their respective complexes [43].
421 This would be expected, as the classic role of NOT1 in eukaryotes is to act as a scaffold upon which effector proteins can
422 be recruited. Moreover, if this hypothesis holds true, another possible mechanism by which PyNOT1-G could function
423 would be to act as a decoy by sufficiently sponging effector proteins away from PyNOT1. However, because the
424 localization and approximate expression levels of PyNOT1 and PyNOT1-G are effectively equal, a stronger interaction
425 between PyNOT1-G and these proteins would be required. Because crosslinking was used in proteomic studies of
426 proteins known to associate with this complex, this permits the detection of direct, short-distance, and long-distance
427 interactions. However, future studies with proximity proteomics approaches could define the spatial and temporal
428 parameters of this complex. Hints as to how these granules may be organized and regulated in *Plasmodium* are perhaps
429 being found in work with yeast. First, a recent study indicated that members of the CCR4/NOT complex are present in
430 processing bodies but were found at lower concentrations and were more dynamic [45]. Additionally, two other studies
431 indicated that the partitioning of Dhh1, the ortholog of DOZI, is adversely affected by the association with NOT1, and
432 positively affected by association with Pat1 [30, 46]. Because no bioinformatically predictable ortholog of Pat1 is present
433 in any *Plasmodium* species, identifying and understanding the regulators of granule assembly and disassembly will
434 require further experimentation.

435 Overall, we conclude that *Plasmodium* and closely related parasites have taken the novel strategy of duplicating NOT1 to
436 allow the dedication of one paralogue for a gametocyte/gamete-specific role in host-to-vector transmission. However,
437 key aspects of how it toggles between its dual natures remain unanswered. As there is an overrepresentation of AU-rich
438 sequences in the *Plasmodium* transcriptome, the role of ELAV/HuR and TTP RNA-binding proteins that typically bind
439 these AU-rich sequences may be diminished. Accordingly, the TTP-binding domain that typically enables their
440 recruitment to the CAF1/CCR4/NOT complex in model eukaryotes and human cells is dispensable for PyNOT1-G's critical

441 functions. Therefore, it is plausible that *Plasmodium* has adopted an alternate strategy by adapting the functions of
442 canonical binding partners, or through the recruitment of additional *Plasmodium*-specific proteins to this unique,
443 transmission-adapted NOT1 paralogue.

444

445 **Materials and Methods:**

446 Ethics Statement

447 All animal care strictly followed the Association for Assessment and Accreditation of Laboratory Animal Care (AAALAC)
448 guidelines and was approved by the Pennsylvania State University Institutional Animal Care and Use Committee (IACUC#
449 PRAMS201342678). All procedures involving vertebrate animals were conducted in strict accordance with the
450 recommendations in the Guide for Care and Use of Laboratory Animals of the National Institutes of Health with
451 approved Office for Laboratory Animal Welfare (OLAW) assurance.

452 Experimental Animals

453 Six-to-eight-week-old female Swiss Webster mice from Envigo were used for all experiments in this work. *Anopheles*
454 *stephensi* mosquitoes were reared at 24 C and 70% humidity and were fed with 0.05% w/v PABA-supplemented 10%
455 w/v sugar water.

456 Production and Confirmation of *Plasmodium yoelii* Transgenic Parasites

457 Transgenic *Plasmodium yoelii* 17XNL strain parasites were produced through conventional reverse genetics approaches
458 using two homology arms that are specific to the targeted gene [47, 48]. Homology arms were PCR amplified from wild-
459 type genomic DNA, were combined into a single PCR amplicon by SOE PCR, were inserted into pCR-Blunt for sequencing,
460 and were finally inserted into a pDEF plasmid for use in *Plasmodium yoelii* parasites. Plasmids used for gene deletion
461 were based upon pSL0444, which replaces the gene sequences with a GFPmut2 expression cassette, a HsDHFR
462 expression cassette, and the plasmid backbone. Plasmids used for appending a C-terminal GFPmut2 tag to a protein
463 were based upon pSL0442, which inserts a the coding sequence for GFPmut2 with the *P. berghei* DHFR 3'UTR, a HsDHFR
464 expression cassette, and the plasmid backbone into that genomic locus. The PyWT-GFP transgenic line (Py0489) has
465 been described previously [14], and the PyWT-mScarlet line (Py1115) was created in an identical manner but substitutes
466 mScarlet coding sequences for those of GFPmut2. Overexpression of the TTP-binding domain of PyNOT1-G was achieved
467 by inserting these coding sequences (AA1-199) upstream of the GFPmut2 sequences of Py0489. The deletion of the TTP-
468 binding domain of PyNOT1-G was achieved by substitution of these coding sequences with those of GFPmut2 in an N-
469 terminal tag format. Primers used to create all amplicons are provided in Supplemental Table 6, and complete plasmid

470 sequences used to create PyWT-GFP, PyWT-mScarlet, *pynot1⁻*, *pynot1-g⁻*, *pynot1::gfp*, *pynot1-g::gfp*, overexpressor of
471 the TTP-binding domain, and the deletion of the TTP-binding domain are provided in Supplemental File 1.

472 Schizonts used for transfections were produced via *ex vivo* cultures and were purified by an Accudenz discontinuous
473 gradient as previously described [49]. Purified parasites enriched in schizonts were transfected with 10ug linearized
474 plasmid using an Amaxa Nucleofector 2b device using either Lonza T-Cell Solution with Program U-033, or with cytomix
475 using Program T-016. Transgenic parasites were selected by pyrimethamine drug cycling in a parental and a transfer
476 mouse. In some cases, parasites were enriched by FACS and/or cloned by limited dilution approaches. The genotype of
477 parasites was determined by PCR across both homology arms for the targeted genomic locus.

478 Production and Accudenz Purification of *P. yoelii* Schizonts and Gametocytes

479 Schizonts that were depleted of rings, trophozoites, and gametocytes were produced through a subtractive magnetic
480 approach. Blood was collected from mice at approximately 1-2% parasitemia into RPMI1640 media, and was passed
481 over a magnetic column (Miltenyi Biotec, LS Columns) to capture late trophozoites, schizonts, and gametocytes by virtue
482 of the magnetic hemozoin present in them. In contrast, rings and early trophozoites flowed through the column and
483 were collected into fresh media. This depletion process was repeated a total of four times, after which no further
484 depletion of gametocytes in the flow through was observed. Parasites were then subjected to *ex vivo* culture for 12-14
485 hours until mature schizonts were visible by Giemsa-stained thin blood smears.

486 Gametocytes were produced by treatment of the mice at 1% parasitemia with 10 mg/L sulfadiazine (VWR, Cat#
487 AAA12370-30) in their drinking water for two days before exsanguination. The blood was placed in 30 mL of pre-warmed
488 RPMI1640 with 20% v/v FBS to prevent activation of gametocytes and was purified using an Accudenz gradient as
489 previously described [14].

490 Live Fluorescence and IFA-Based Microscopy

491 PyNOT1 and PyNOT1-G expression in blood stages, oocyst sporozoites, salivary gland sporozoites and liver stages was
492 investigated by an indirect immunofluorescence assay (IFA), and expression in day seven oocysts was observed by live
493 fluorescence microscopy. All samples for IFA were prepared as previously described [47]. Parasites were stained with
494 the following primary antibodies: rabbit anti-GFP (1:1000, Invitrogen, Cat# A11122; 1:1000, Pocono Rabbit Farm &
495 Laboratory, Custom polyclonal antibody), rabbit anti-PyACP (1:1000, Pocono Rabbit Farm & Laboratory, Custom
496 polyclonal antibody), mouse anti-GFP (1:1000, DSHB, Clone 4C9), rabbit anti-HsDDX6 that cross-reacts with DOZI
497 (1:1000, gift from Joe Reese, Custom PAb), mouse anti-alpha-tubulin (Clone B-5-1-2) (1:1000, Sigma, Cat# T5168), and
498 mouse anti-PyCSP (1:1000, Clone 2F6 [50]). Secondary antibodies used for all stages were Alexa Fluor-conjugated
499 (AF488, AF594) and specific to rabbit or mouse (1:1000, Invitrogen, Cat# A11001, A11005, A11008, A11012). 4',6-
500 diamidino-2-phenylindole (DAPI) was used to stain nucleic acids following washing away unbound secondary antibodies

501 and samples were covered with VectaShield anti-fade reagent (Vector Laboratories, VWR, Cat# 101098-048) and a
502 coverslip, then sealed with nail polish before visualization. Fluorescence and DIC images were taken using a Zeiss
503 fluorescence/phase contrast microscope (Zeiss Axioscope A1 with 8-bit AxioCam ICc1 camera) using a 40X or 100X oil
504 objective and processed by Zen imaging software.

505 RNA-seq Sample Production, Data Analysis and Interpretation

506 RNA from *P. yoelii* asexual blood stage schizonts or gametocytes was prepared using the Qiagen RNeasy kit with two
507 sequential DNaseI on-column digests, with quality control analysis by BioAnalyzer. Samples were used to create
508 barcoded libraries (Illumina TruSeq Stranded mRNA Library) and were sequenced on an Illumina HiSeq 2500 to yield 100
509 nt long single end reads for each of three biological replicates per sample type. These data were mapped to the *P. yoelii*
510 reference genome (*P. yoelii* 17XNL strain, plasmodb.org v50) using hisat2 (version 2.1.0) [51] specifying --rna-strandness
511 R and --max-intronlen 5000 parameters. Coverage files were generated and the mapped data was visualized and
512 manually inspected in Integrative Genomics Viewer (IGV) as a quality control check [52]. Reads that mapped to
513 annotated genes (PlasmoDB.org v50) were counted using featureCounts (version 2.0.0) [53] and specified –s 2 –t exon –
514 g gene_id parameters. The raw read counts were normalized with DESeq2 (version 1.26.0) [54], which was also used to
515 determine the differentially expressed genes between the sample types. The Transcript Integrity Number (TIN) [40] for
516 each gene was calculated and used to further filter out the differentially expressed genes that do not have coverage
517 evenness across the entire length of the gene as described before [39]. Briefly, TIN was calculated from the
518 transcriptome as built from the annotation files and pseudobam files as generated using Kallisto (version 0.46.1,
519 parameters used: specifying --rf-stranded --single -l 150 -s 20 -b 10) [55]. The samtools depth command was used to
520 determine read depth at each position in the transcript and TIN was calculated as previously described [55]. Custom
521 python scripts are provided as Supplemental File 3. For genes with multiple transcripts, the maximum of the transcript
522 TINs was considered as the integrity value for the gene. Differentially expressed genes with FDR <0.05 were flagged for
523 inspection if the read count is >20 in either of the conditions but TIN is <40 in both conditions. TIN-$\log_2$-fold change was
524 calculated, and the flagged genes were resolved and included in the differential expression set if the absolute value of
525 TIN log2-FC is <=1.5. For genes with read count >20 and TIN <40, transcript overlap from neighboring genes were
526 checked using a custom python script (Supplemental File 3) and were flagged if an overlap was detected. A MakeFile
527 describing the complete bioinformatics workflow (including all steps noted above) and other scripts used are also
528 provided in Supplemental File 3. Gene ontology terms (cellular components, molecular functions, and biological
529 processes) were retrieved from PlasmoDB.org (v51). RNA-seq data reported here is available through the GEO
530 depository (Accession #GSE136674). To generate a heatmap, sample raw counts were transformed using variance
531 stabilizing transformation (vst) function and the Euclidean distance between the samples were computed using dist
532 function in R. These were then clustered with complete-linkage algorithm implemented in the pheatmap package in R.
533 Coloring scale shows the distance between samples. Samples are listed in the same order for both rows (top to bottom)

534 and columns (left to right). A PCA plot was generated with the plotPCA function available in DESeq2 package, using vst
535 with transformed raw counts as the input. To generate MA plots, shrunken log2 fold changes were estimated using
536 adaptive shrinkage estimator from the ashr package [56]. These were then visualized with plotMA function in
537 DESeq2 package. Points are colored red if the adjusted p value is less than 0.05. Data points that fall out of these limits
538 are plotted as open triangles pointing either up or down.

539 Measurement of Asexual Growth Kinetics and Male Gametocyte Activation

540 Cryopreserved blood infected with either *P. yoelii* wild-type (Py17XNL strain) or transgenic parasites was injected
541 intraperitoneally into Swiss Webster starter mice, and parasitemia was allowed to increase to 1%. This blood was
542 extracted via cardiac puncture and diluted in RPMI to 1,000 parasites per 100ul microliters. One hundred microliters was
543 injected intravenously (IV) into three mice for each of three biological replicates for each parasite line. Parasitemia was
544 measured daily by Giemsa-stained thin blood smears, and male gametocyte activation was monitored daily by counting
545 exflagellation centers ("centers of movement") via wet mount of a drop of blood incubated at room temperature for 8
546 minutes as previously described [21].

547 Measurement of Differences in Gametocytemia by Flow Cytometry

548 Comparisons of gametocyte numbers were made using flow cytometry. Briefly, three experimental mice were infected
549 with 1,000 PyWT-GFP or *pynot1-g*$^{-}$ (GFP+) parasites by IV injection as described above. The parasitemia was monitored
550 daily, and upon reaching 1% parasitemia, the mice were treated with sulfadiazine for 2 days to selectively kill asexual
551 blood stage parasites. Blood was collected by cardiac puncture and the fraction of GFP+ cells were counted on a
552 Beckman Coulter Astrios Moflo EQ (Brea, CA) in tube mode using uninfected blood and *P. yoelii* 17XNL wild-type
553 parasite-infected blood as negative controls. All data was analyzed by FlowJo (v10.6.1).

554 Mosquito Transmission

555 Swiss Webster (SW) mice were infected with *P. yoelii* wild-type or transgenic parasites by IP or IV injection as previously
556 described [21]. Mice were screened daily for parasitemia and the presence of male gametocyte activation (centers of
557 movement). On the timepoints indicated, the mice were anesthetized by IP injection of a ketamine/xylazine cocktail and
558 were exposed to mosquitoes for 15 minutes with their positions adjusted every 5 minutes to allow for more even
559 feeding. Mosquito transmission was assessed by dissection of a minimum of 50 midguts on day seven post-blood meal,
560 which were analyzed for the prevalence of infection and oocyst numbers by DIC and fluorescence microscopy.

561 Genetic Crosses

562 WT (Colorless) vs *pynot1-g*$^{-}$ (GFP+) Genetic Cross: Blood from mice infected with either Py17XNL wild-type parasites or
563 *pynot1-g*$^{-}$ transgenic parasites was serially diluted to 5,000 infected RBCs per 50ul, and was used to infect groups of
564 three experimental mice with either 10,000 wild-type parasites, 5,000 wild-type parasites and 5000 *pynot1-g*$^{-}$ transgenic
565 parasites, or 10,000 *pynot1-g*$^{-}$ transgenic parasites in biological triplicate. Parasitemia and male gametocyte activation
566 were monitored daily, and mice were fed to mosquitoes as above on the day indicated. Midguts were analyzed on day
567 seven post-blood meal on a fluorescence microscope as above, and numbers of oocysts and their fluorescence were
568 recorded (Green or colorless).

569 PyWT-mScarlet, PyWT-GFP, *pynot1-g*$^{-}$ (GFP+): Blood from mice infected with either Py17XNL wild-type parasites
570 expressing mScarlet (PyWT-mScarlet, Py1115) or GFPmut2 (PyWT-GFP, Py489) or *pynot1-g*$^{-}$ transgenic parasites was
571 collected by cardiac puncture and combined for *in vitro* ookinete cultures as previously described [57, 58]. Briefly, blood
572 was collected on the peak day of exflagellation for Py489 and/or Py1115 (as male *pynot1-g*$^{-}$ transgenic parasites do not
573 complete gametogenesis and do not exflagellate) when the parasitemia was each of the mice was comparable. Blood
574 from each infected mouse was added to 30 ml iRPMI (RPMI with HEPES and L- glutamine; no FBS), and infected red
575 blood cells were enriched by an Accudenz gradient as described above. The parasitized cells were collected from the
576 interface and resuspended in iRPMI. For genetic cross experiments, equal volumes of resuspended parasites at
577 comparable parasitemia were either added alone or in combination with another parasite line to 10 ml *in vitro* ookinete
578 media (RPMI with HEPES and L-glutamine, 20% FBS (Corning, Prod No. 35-011-CV, Lot No. 35011126), 0.05% w/v
579 hypoxanthine, 100 uM xanthurenic acid, pH 8.2) and were allowed to develop at room temperature for 24 hours.
580 Parasites were assessed by live fluorescence microscopy for mScarlet and/or GFPmut2 expression as described above.

581 Statistical Analyses

582 Statistical tests for RNA-seq analyses and comparisons were provided by DEseq2 [54]. The statistical test assessments of
583 GO terms (Odds Ratio, P-value, Benjamini, Bonferroni) were provided by PlasmoDB.org (v51). All other statistical tests
584 were conducted with GraphPad Prism (v9) with the specific test(s) used noted where applied.

585 Data Availability Statement

586 RNA-seq datasets, including the raw and processed transcriptomic files (including DESeq2 output files), have been
587 deposited at GEO (Accession # GSE136674). The complete bioinformatics workflow (MakeFile) and the scripts used in
588 RNA-seq data processing are provided as Supplemental File 3.

589

590 Acknowledgments

591 We acknowledge Andy Waters for helpful discussions in the depletion of gametocytes from mixed blood stage parasites,
592 and Katarzyna Modrzynska for advice on the optimization of *in vitro* ookinete cultures. We are grateful to Sarah Neering
593 and Brian Dawson for assistance with flow cytometry data collection and analysis, as well as to the Penn State Genomics
594 and Flow Cytometry Facilities operated by the Huck Institutes of the Life Sciences, University Park, PA. We acknowledge
595 and appreciate the critical guidance from Istvan Albert on the processing and analysis of RNA-seq datasets. Finally, we
596 thank members of the Lindner and Llinás laboratories for critical discussions and evaluations of this manuscript.

597 Funding

598 This work was supported by an R01 from the National Institutes of Allergy and Infectious Diseases (R01AI123341 to SEL).

599 Conflict of Interest

600 The authors declare that they have no conflict of interest.

601

602 **Figure and Table Legends:**

603 **Figure 1: NOT1 is Duplicated in the Aconoidasida Class of Apicomplexans.** Shown here are examples of NOT1 proteins
604 from the Aconoidasida class of apicomplexans with a representative model eukaryote NOT1 protein from *S. cerevisiae*.
605 Protein and domain sizes are drawn to scale. Bioinformatically predicted domains were identified through BlastP
606 searches and amino acid alignments.

607 **Figure 2: PyNOT1 and PyNOT1-G have similar expression patterns and localize to cytosolic puncta.** Representative IFA
608 images of (A) PyNOT1::GFP and (B) PyNOT1-G::GFP blood stage parasites show localization patterns typical for the
609 CAF1/CCR4/NOT complex in eukaryotes. All samples were stained with DAPI and mouse anti-GFP to image PyNOT1::GFP
610 or PyNOT1-G::GFP. Asexual blood stage parasites were counterstained with anti-PyACP and DAPI to identify ring,
611 trophozoite, and schizont stages. Gametocytes were counterstained with anti-alpha tubulin (male) or anti-PyCITH
612 (female). Scale bar is 5 microns.

613 **Figure 3: PyNOT1-G is essential to the formation of male gametes.** (A) The blood stage growth of Py17XNL wild-type
614 parasites and two independent clones of *pynot1-g*$^-$ parasites was compared over the entire course of infection in
615 biological triplicate, with each replicate done in technical triplicate. Maximal parasitemia of *pynot1-g*$^-$ parasites was
616 lower and resulted in slightly faster clearance by the mouse. (B) The number of gametocytes produced by Py17XNL WT-
617 GFP parasites and two independent clones of *pynot1-g*$^-$ parasites was measured by flow cytometry using the presence of
618 GFP fluorescence in biological duplicate, with each replicate done in technical triplicate. Average values for each
619 biological replicate, their median and range are provided. Statistical comparisons used an unpaired t test with Welch
620 correction. (C) Male gametogenesis was measured by DIC microscopy to count the number of exflagellation centers
621 ("centers of movement") per microscopic field using a 10x eyepiece and 40x objective lens. The same mice and
622 timepoints were used as in panel A, and were assessed in biological triplicate, with each replicate done in technical
623 triplicate. A cross symbol (A, C) indicates that a single mouse infected with Py17XNL wild-type parasites was euthanized
624 on day 15 due to parasitemia more than 10% as required by our approved vertebrate animal protocols. Error bars
625 indicate the standard deviation.

626 **Figure 4: PyNOT1-G is essential to the development of zygotes resulting from female gametocytes.** (A) A genetic cross
627 experiment with Py17XNL wild-type parasites (colorless) and *pynot1-g*$^-$ (GFP+) transgenic parasites was conducted to
628 assess effects upon parasite transmission. Mice were infected with a total of 10,000 mixed blood stage parasites
629 consisting of only wild-type parasites, an equal mixture of wild-type and transgenic parasites, or only transgenic
630 parasites. Mosquito transmission occurred on the day where peak exflagellation was observed for mice infected with
631 only wild-type parasites, and colorless and GFP+ oocysts were counted seven days post-blood meal by fluorescence and
632 DIC microscopy. An illustration of the experimental readout/interpretation (top) and the results (bottom) are provided.

633 Experiments were conducted in biological triplicate, with error bars denoting SEM. (B) A genetic cross experiment with
634 Py17XNL WT-mScarlet, WT-GFP, and *pynot1-g*$^-$ (GFP+) transgenic parasites was conducted using *in vitro* ookinete culture
635 conditions. Equal volumes of infected blood at comparable parasitemias were mixed as indicated and were scored by
636 live fluorescence microscopy for the presence/absence of mScarlet and GFP signals. Representative images of the WT-
637 mScarlet x WT-GFP genetic cross are provided to show zygote, retort, and ookinete stages (top). Results of all tested
638 genetic crosses are provided (bottom) from experiments conducted in biological duplicate. Parasites resulting from the
639 WT-mScarlet x *pynot1-g*$^-$ (GFP+) cross could not develop beyond the zygote stage. Scale bars are 5 microns (zygote,
640 retort) or 10 microns (ookinete).

641 **Figure 5: Extensive dysregulation of mRNAs in *pynot1-g*$^-$ schizonts and gametocytes.** Comparative RNA-seq of wild-type
642 or *pynot1-g*$^-$ transgenic parasites was conducted using mixed male and female gametocytes or schizonts that were
643 enriched through a subtractive magnetic depletion approach. (A) A heatmap showing the Euclidean distance between
644 samples was generated from the raw counts transformed using the vst function. Samples are ordered the same for both
645 rows (top to bottom) and columns (left-to-right). (B) These transformed raw counts were also used as the input values to
646 generate a PCA plot to demonstrate sample clustering. (C and D) MA plots generated from the estimated shrunken $\log_2$
647 fold changes are shown for gametocytes (C) and schizonts (D), with data points shaded in red indicating $p < 0.05$. Data
648 points that do not meet this threshold are denoted as open triangles (oriented up or down). (E and F) Plotted are the -
649 Log_{10} false discovery rate (FDR) vs the Log_2 Fold Change values for differentially expressed transcripts as per DEseq2,
650 with transcripts shaded based upon their fold change values. Similar gametocyte- and early mosquito stage-enriched
651 transcripts were significantly lower in abundance in both stages.

652 **Figure 6: The putative tristetraproline-binding domain is dispensable for all essential blood stage functions of**
653 **PyNOT1-G.** Clonal transgenic parasites overexpressing the predicted tristetraproline-binding domain fused to GFP
654 (TTPbd::GFP) from the safe harbor *p230p* genomic locus were compared to Py17XNL WT-GFP parasites for (A) asexual
655 blood stage growth and (B) male gametogenesis. Clonal transgenic parasites expressing a variant of PyNOT1-G where
656 the N-terminal TTPbd has been replaced with GFP were compared to Py17XNL WT-GFP parasites for (C) asexual blood
657 stage growth and (D) male gametogenesis. A cross symbol (A, B) indicates that a single mouse infected with TTPbd::GFP
658 Clone 2 parasites was euthanized on day 15 due to parasitemia more than 10% as required by our approved vertebrate
659 animal protocols. Error bars indicate the standard deviation.

660 **Figure 7: A proposed composite interaction network of NOT1-G.** Crosslinking IP datasets for PbDOZI and PbCITH
661 (orange lines), PyCCR4-1 (green lines), and PyALBA4 (light blue lines) were used to propose a composite interaction
662 network with PyNOT1-G. The placement of some proteins is based upon known direct interactions from the literature
663 (e.g. NOT1-G, CAF1, CCR4, CAF40, NOT4, NOT2, NOT5, PABP1, CELF2, DOZI, eIF4F (eIF4E, eIF4A, eIF4G), as are the
664 placements of the 5' m7G cap next to the cap-binding protein eIF4E and the poly(A) tail with PABP1. Deletion

665 phenotypes for *pynot1-g* match or exceed those of *pbdozi*$^{-}$, *pyccr4-1*$^{-}$, and the *pycaf1* truncation, and lead to a complete
666 arrest in male parasite development and in development of female parasites beyond the zygote stage.

667

668 **Supplemental Figure Legends:**

669 **Supplemental Figure 1: Genotyping PCR of PyNOT1::GFP and PyNOT1-G::GFP transgenic parasites.** Genomic DNA from
670 transgenic parasites was compared to that of Py17XNL wild-type parasites or no template controls by genotyping PCR. A
671 schematic of the wild-type and designed transgenic loci are provided below each gel image. Primers used are identified
672 in Supplemental Table 6 for assessing (A) PyNOT1::GFP and (B) PyNOT1-G::GFP parasites. (A) The PSU 1kb molecular
673 weight (MW) ladder [59] or the NEB 1kb+ molecular weight (MW) ladder (B) flanks all experimental lanes.

674 **Supplemental Figure 2: PyNOT1 and PyNOT1-G have similar expression patterns throughout mosquito stage**
675 **development.** The expression of PyNOT1::GFP and PyNOT1-G::GFP in mosquito stage were assessed by live fluorescence
676 (day 7 oocysts) or by IFA (day 10 oocyst sporozoites, day 14 salivary gland sporozoites). Sporozoites were counterstained
677 with anti-PyCSP and DAPI. Scale bar is 20 microns (oocyst) or 10 microns (sporozoites).

678 **Supplemental Figure 3: Genotyping PCR of *pynot1*$^{-}$ and *pynot1-g*$^{-}$ transgenic parasites.** Genomic DNA from (A) *pynot1*$^{-}$
679 or (B) *pynot1-g*$^{-}$ transgenic parasites was compared to that of Py17XNL wild-type parasites or no template controls by
680 genotyping PCR. A schematic of the wild-type and designed transgenic loci are provided below each gel image. Primers
681 used are identified in Supplemental Table 6. (A) The NEB 1kb+ molecular weight (MW) ladder (B) flanks all experimental
682 lanes.

683 **Supplemental Figure 4: Genotyping PCR and western blotting of TTPbd::GFP overexpression parasites and ΔTTPbd**
684 **transgenic parasites. (A, C)** Genomic DNA from transgenic parasites was compared to that of Py17XNL wild-type
685 parasites or no template controls by genotyping PCR. A schematic of the wild-type and designed transgenic loci are
686 provided below each gel image. (B) Western blotting of TTPbd::GFP vs Py17XNL WT-GFP parasite lysate enriched by
687 immunoprecipitation with anti-GFP is shown (I = Input, FT = Flow Through, E = Elution). Primers used are identified in
688 Supplemental Table 6 for assessing (A) PyNOT1-G TTPbd::GFP at the *p230p* genomic locus and (B) PyNOT1-G::GFP
689 parasites. (A) The PSU 1kb molecular weight (MW) ladder [59] or the NEB 1kb+ molecular weight (MW) ladder (C) flanks
690 all experimental lanes.

691

692 **Supplemental Table Descriptions:**

693 **Supplemental Table 1:** Processed RNA-seq data for gametocyte samples comparing Py17XNL wild-type parasites and
694 *pynot1-g*$^{-}$ transgenic parasites as conducted in biological triplicate.

695 **Supplemental Table 2:** Overlapping genes that are similarly dysregulated in *pynot1-g*$^{-}$, *pyalba4*$^{-}$, *pbdozi*$^{-}$, and *pbcith*$^{-}$
696 transgenic parasites.

697 **Supplemental Table 3:** Processed RNA-seq data for asexual blood stage schizont samples comparing Py17XNL wild-type
698 parasites and *pynot1-g*$^{-}$ transgenic parasites as conducted in biological triplicate.

699 **Supplemental Table 4:** Transmission data for Py17XNL WT-GFP parasites (Py489) and PyNOT1-G TTPbd::GFP
700 overexpression parasites (Py1125).

701 **Supplemental Table 5:** Comparisons of immunoprecipitation/mass spectrometry-based proteomic datasets for PyCCR4-
702 1, PyALBA4, and PbDOZI/PbCITH (related to Figure 7).

703 **Supplemental Table 6:** Oligonucleotides used in this study.

704

705 **Supplemental File Descriptions:**

706 **Supplemental File 1:** Complete sequences for plasmids used in this study.

707 **Supplemental File 2:** Flow cytometry panels obtained during the measurement of gametocytemia of PyWT-GFP and
708 *pynot1-g*$^{-}$ transgenic parasites (Related to Figure 3B).

709 **Supplemental File 3:** A Makefile log of complete RNA-seq bioinformatics workflow, along with all custom R and python
710 scripts used in this work.

711

712 **References**

713 1. *World Health Organization, World Malaria Report*. 2020.
714 2. Lindner, S.E., J.L. Miller, and S.H. Kappe, *Malaria parasite pre-erythrocytic infection: preparation meets*
715 *opportunity.* Cell Microbiol, 2012. **14**(3): p. 316-24.
716 3. Sturm, A., et al., *Manipulation of host hepatocytes by the malaria parasite for delivery into liver sinusoids.*
717 Science, 2006. **313**(5791): p. 1287-90.
718 4. Josling, G.A., et al., *Dissecting the role of PfAP2-G in malaria gametocytogenesis.* Nat Commun, 2020. **11**(1): p.
719 1503.
720 5. Kafsack, B.F., et al., *A transcriptional switch underlies commitment to sexual development in malaria parasites.*
721 Nature, 2014. **507**(7491): p. 248-52.
722 6. Sinha, A., et al., *A cascade of DNA-binding proteins for sexual commitment and development in Plasmodium.*
723 Nature, 2014. **507**(7491): p. 253-257.
724 7. Singh, S., et al., *The PfAP2-G2 transcription factor is a critical regulator of gametocyte maturation.* Mol
725 Microbiol, 2020.
726 8. Modrzynska, K., et al., *A Knockout Screen of ApiAP2 Genes Reveals Networks of Interacting Transcriptional*
727 *Regulators Controlling the Plasmodium Life Cycle.* Cell Host Microbe, 2017. **21**(1): p. 11-22.
728 9. Yuda, M., et al., *Global transcriptional repression: An initial and essential step for Plasmodium sexual*
729 *development.* Proc Natl Acad Sci U S A, 2015. **112**(41): p. 12824-9.
730 10. Josling, G.A., K.C. Williamson, and M. Llinas, *Regulation of Sexual Commitment and Gametocytogenesis in*
731 *Malaria Parasites.* Annu Rev Microbiol, 2018. **72**: p. 501-519.
732 11. Rea, E., K.G. Le Roch, and R. Tewari, *Sex in Plasmodium falciparum: Silence Play between GDV1 and HP1.* Trends
733 Parasitol, 2018. **34**(6): p. 450-452.
734 12. Reddy, B.P., et al., *A bioinformatic survey of RNA-binding proteins in Plasmodium.* BMC Genomics, 2015. **16**: p.
735 890.
736 13. Rios, K.T. and S.E. Lindner, *Protein-RNA interactions important for Plasmodium transmission.* PLoS Pathog, 2019.
737 **15**(12): p. e1008095.
738 14. Munoz, E.E., et al., *ALBA4 modulates its stage-specific interactions and specific mRNA fates during Plasmodium*
739 *yoelii growth and transmission.* Mol Microbiol, 2017. **106**(2): p. 266-284.
740 15. Shrestha, S., et al., *The RNA-binding protein Puf1 functions in the maintenance of gametocytes in Plasmodium*
741 *falciparum.* J Cell Sci, 2016. **129**(16): p. 3144-52.
742 16. Guerreiro, A., et al., *Genome-wide RIP-Chip analysis of translational repressor-bound mRNAs in the Plasmodium*
743 *gametocyte.* Genome Biol, 2014. **15**(11): p. 493.
744 17. Miao, J., et al., *Puf mediates translation repression of transmission-blocking vaccine candidates in malaria*
745 *parasites.* PLoS Pathog, 2013. **9**(4): p. e1003268.
746 18. Miao, J., et al., *The Puf-family RNA-binding protein PfPuf2 regulates sexual development and sex differentiation*
747 *in the malaria parasite Plasmodium falciparum.* J Cell Sci, 2010. **123**(Pt 7): p. 1039-49.
748 19. Mair, G.R., et al., *Universal features of post-transcriptional gene regulation are critical for Plasmodium zygote*
749 *development.* PLoS Pathog, 2010. **6**(2): p. e1000767.
750 20. Mair, G.R., et al., *Regulation of sexual development of Plasmodium by translational repression.* Science, 2006.
751 **313**(5787): p. 667-9.
752 21. Hart, K.J., et al., *Plasmodium male gametocyte development and transmission are critically regulated by the two*
753 *putative deadenylases of the CAF1/CCR4/NOT complex.* PLoS Pathog, 2019. **15**(1): p. e1007164.
754 22. Collart, M.A., *The Ccr4-Not complex is a key regulator of eukaryotic gene expression.* Wiley Interdiscip Rev RNA,
755 2016. **7**(4): p. 438-54.
756 23. Ukleja, M., et al., *The architecture of the Schizosaccharomyces pombe CCR4-NOT complex.* Nat Commun, 2016.
757 **7**: p. 10433.
758 24. Collart, M.A. and O.O. Panasenko, *The Ccr4-Not Complex: Architecture and Structural Insights.* Subcell Biochem,
759 2017. **83**: p. 349-379.
760 25. Radhakrishnan, A., et al., *The DEAD-Box Protein Dhh1p Couples mRNA Decay and Translation by Monitoring*
761 *Codon Optimality.* Cell, 2016. **167**(1): p. 122-132 e9.

762 26. Parker, R., *RNA degradation in Saccharomyces cerevisae.* Genetics, 2012. **191**(3): p. 671-702.
763 27. Lai, W.S., et al., *Importance of the Conserved Carboxyl-Terminal CNOT1 Binding Domain to Tristetraprolin*
764 *Activity In Vivo.* Mol Cell Biol, 2019. **39**(13).
765 28. Mukherjee, N., et al., *Global target mRNA specification and regulation by the RNA-binding protein ZFP36.*
766 Genome Biol, 2014. **15**(1): p. R12.
767 29. Buschauer, R., et al., *The Ccr4-Not complex monitors the translating ribosome for codon optimality.* Science,
768 2020. **368**(6488).
769 30. Mugler, C.F., et al., *ATPase activity of the DEAD-box protein Dhh1 controls processing body formation.* Elife,
770 2016. **5**.
771 31. Balu, B., et al., *CCR4-associated factor 1 coordinates the expression of Plasmodium falciparum egress and*
772 *invasion proteins.* Eukaryot Cell, 2011. **10**(9): p. 1257-63.
773 32. Sayers, E.W., et al., *Database resources of the National Center for Biotechnology Information.* Nucleic Acids Res,
774 2021. **49**(D1): p. D10-D17.
775 33. Warrenfeltz, S., et al., *EuPathDB: The Eukaryotic Pathogen Genomics Database Resource.* Methods Mol Biol,
776 2018. **1757**: p. 69-113.
777 34. Koonin, E.V., *Orthologs, paralogs, and evolutionary genomics.* Annu Rev Genet, 2005. **39**: p. 309-38.
778 35. Kedersha, N., et al., *Stress granules and processing bodies are dynamically linked sites of mRNP remodeling.* J
779 Cell Biol, 2005. **169**(6): p. 871-84.
780 36. Zhang, M., et al., *Uncovering the essential genes of the human malaria parasite Plasmodium falciparum by*
781 *saturation mutagenesis.* Science, 2018. **360**(6388).
782 37. Bushell, E., et al., *Functional Profiling of a Plasmodium Genome Reveals an Abundance of Essential Genes.* Cell,
783 2017. **170**(2): p. 260-272 e8.
784 38. Schwach, F., et al., *PlasmoGEM, a database supporting a community resource for large-scale experimental*
785 *genetics in malaria parasites.* Nucleic Acids Res, 2015. **43**(Database issue): p. D1176-82.
786 39. Lindner, S.E., et al., *Transcriptomics and proteomics reveal two waves of translational repression during the*
787 *maturation of malaria parasite sporozoites.* Nat Commun, 2019. **10**(1): p. 4964.
788 40. Wang, L., et al., *Measure transcript integrity using RNA-seq data.* BMC Bioinformatics, 2016. **17**: p. 58.
789 41. Kent, R.S., et al., *Inducible developmental reprogramming redefines commitment to sexual development in the*
790 *malaria parasite Plasmodium berghei.* Nat Microbiol, 2018. **3**(11): p. 1206-1213.
791 42. Vembar, S.S., et al., *The PfAlba1 RNA-binding protein is an important regulator of translational timing in*
792 *Plasmodium falciparum blood stages.* Genome Biol, 2015. **16**: p. 212.
793 43. Liu, Y., et al., *Antagonistic roles of NOT1 paralogues in the timing of gene expression in Plasmodium*
794 *falciparum.* bioRxiv, 2020: p. 2020.02.12.945477.
795 44. Schulz, K.N. and M.M. Harrison, *Mechanisms regulating zygotic genome activation.* Nat Rev Genet, 2019. **20**(4):
796 p. 221-234.
797 45. Xing, W., et al., *A quantitative inventory of yeast P body proteins reveals principles of composition and specificity.*
798 Elife, 2020. **9**.
799 46. Sachdev, R., et al., *Pat1 promotes processing body assembly by enhancing the phase separation of the DEAD-box*
800 *ATPase Dhh1 and RNA.* Elife, 2019. **8**.
801 47. Bowman, L.M., et al., *Definition of constitutive and stage-enriched promoters in the rodent malaria parasite,*
802 *Plasmodium yoelii.* Malar J, 2020. **19**(1): p. 424.
803 48. Jongco, A.M., et al., *Improved transfection and new selectable markers for the rodent malaria parasite*
804 *Plasmodium yoelii.* Mol Biochem Parasitol, 2006. **146**(2): p. 242-50.
805 49. Lindner, S.E., et al., *Perturbations of Plasmodium Puf2 expression and RNA-seq of Puf2-deficient sporozoites*
806 *reveal a critical role in maintaining RNA homeostasis and parasite transmissibility.* Cell Microbiol, 2013. **15**(7): p.
807 1266-83.
808 50. Lindner, S.E., et al., *Total and putative surface proteomics of malaria parasite salivary gland sporozoites.* Mol Cell
809 Proteomics, 2013. **12**(5): p. 1127-43.
810 51. Kim, D., B. Langmead, and S.L. Salzberg, *HISAT: a fast spliced aligner with low memory requirements.* Nat
811 Methods, 2015. **12**(4): p. 357-60.
812 52. Robinson, J.T., et al., *Integrative genomics viewer.* Nat Biotechnol, 2011. **29**(1): p. 24-6.

813 53. Liao, Y., G.K. Smyth, and W. Shi, *featureCounts: an efficient general purpose program for assigning sequence*
814 *reads to genomic features.* Bioinformatics, 2014. **30**(7): p. 923-30.
815 54. Love, M.I., W. Huber, and S. Anders, *Moderated estimation of fold change and dispersion for RNA-seq data with*
816 *DESeq2.* Genome Biol, 2014. **15**(12): p. 550.
817 55. Bray, N.L., et al., *Near-optimal probabilistic RNA-seq quantification.* Nat Biotechnol, 2016. **34**(5): p. 525-7.
818 56. Stephens, M., *False discovery rates: a new deal.* Biostatistics, 2017. **18**(2): p. 275-294.
819 57. Moon, R.W., et al., *A cyclic GMP signalling module that regulates gliding motility in a malaria parasite.* PLoS
820 Pathog, 2009. **5**(9): p. e1000599.
821 58. Janse, C.J., et al., *In vitro formation of ookinetes and functional maturity of Plasmodium berghei gametocytes.*
822 Parasitology, 1985. **91 (Pt 1)**: p. 19-29.
823 59. Henrici, R.C., et al., *The pPSU Plasmids for Generating DNA Molecular Weight Markers.* Sci Rep, 2017. **7**(1): p.
824 2438.

825

826

827 **Table 1: Deletion of the TTP-binding domain of PyNOT1-G is important but dispensable for parasite transmission.**

	WT-GFP (Py0489)	ΔTTPbd Clone 1 (Py1299)	ΔTTPbd Clone 2 (Py1299)
Prevalence of Infection	91.7% / 77.4% / 59.5%	2.9% / 8.8% / 24.7%	3.2% / 31.8% / 42.6%
Average Oocysts/ Infected Mosquito	15.9 / 42.8 / 10.7	3.0 / 7.0 / 11.9	5.0 / 39.5 / 21.8

828

Hart *et al.* Figure 1

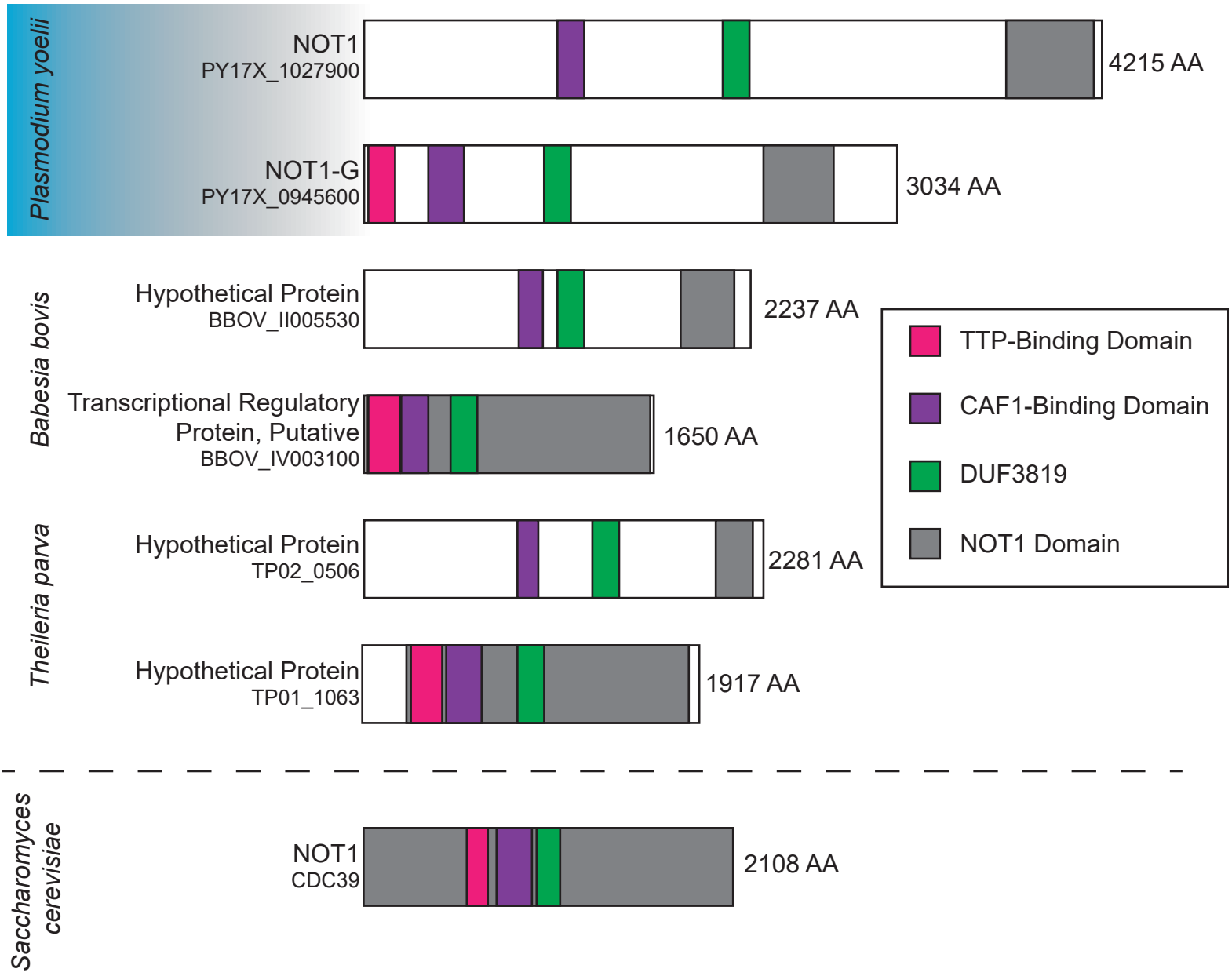

Hart *et al.* Figure 2

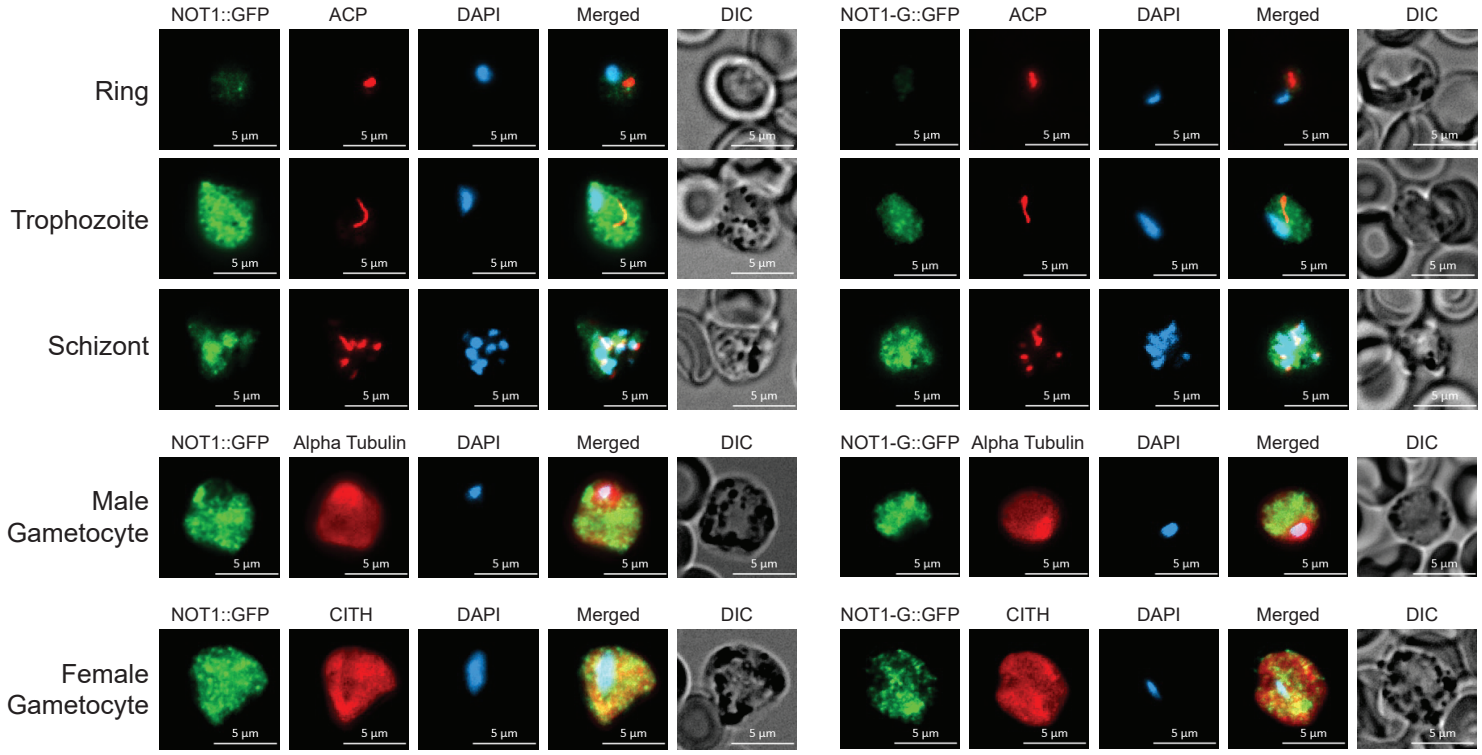

Hart *et al.* Figure 3

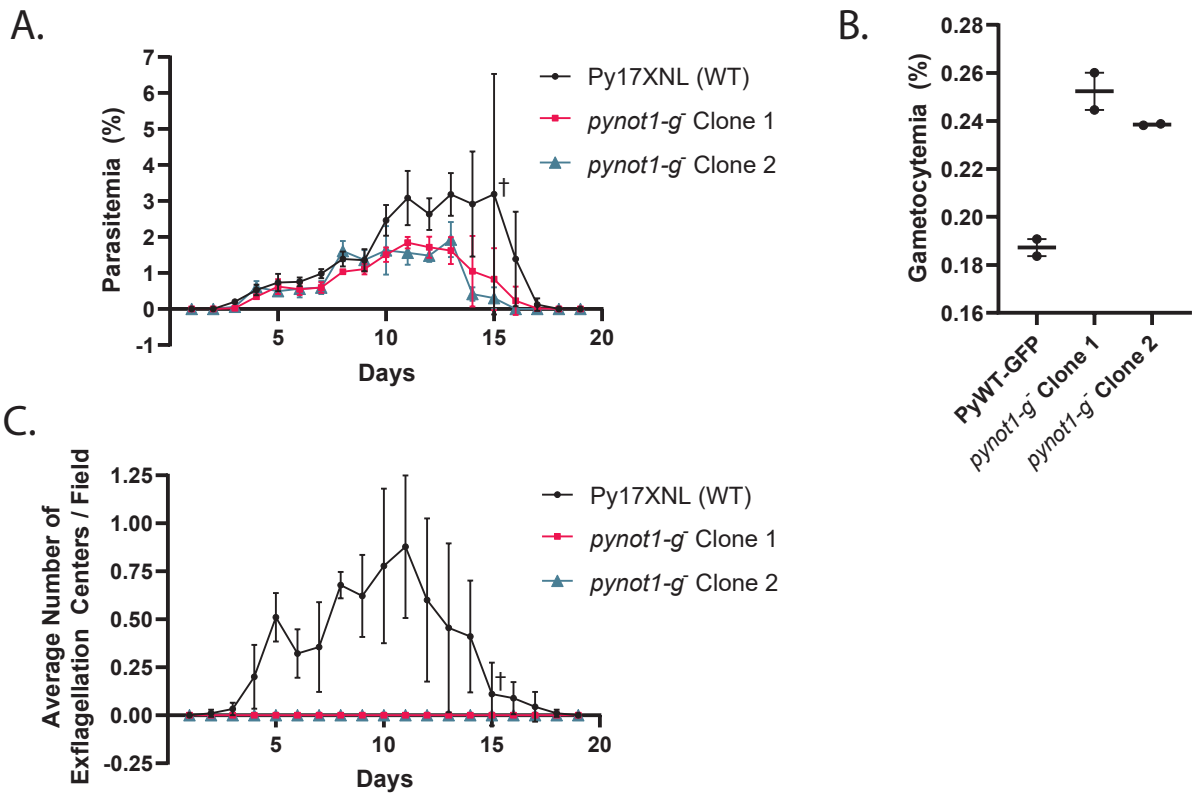

Hart *et al.* Figure 4

A.

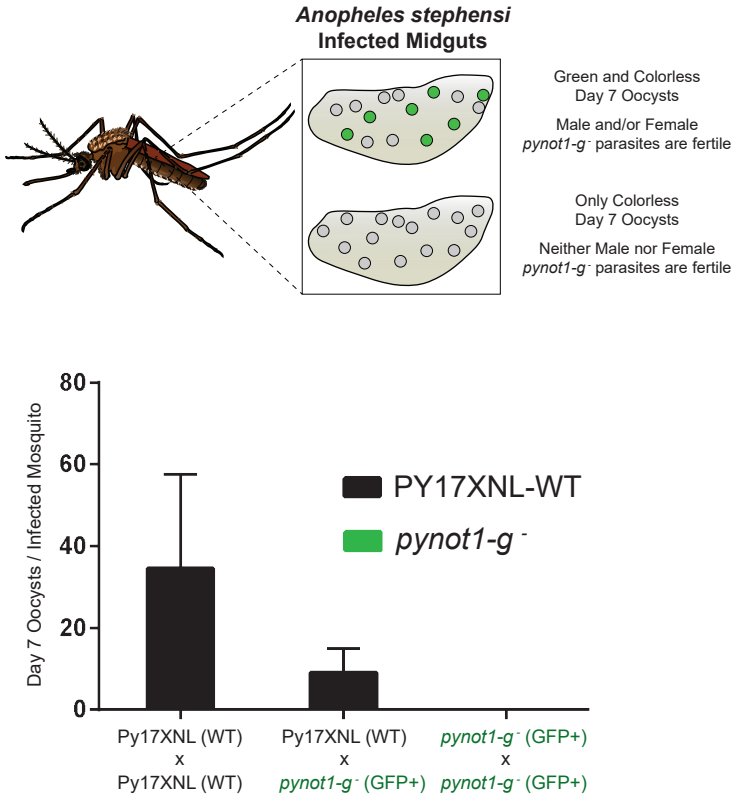

B.

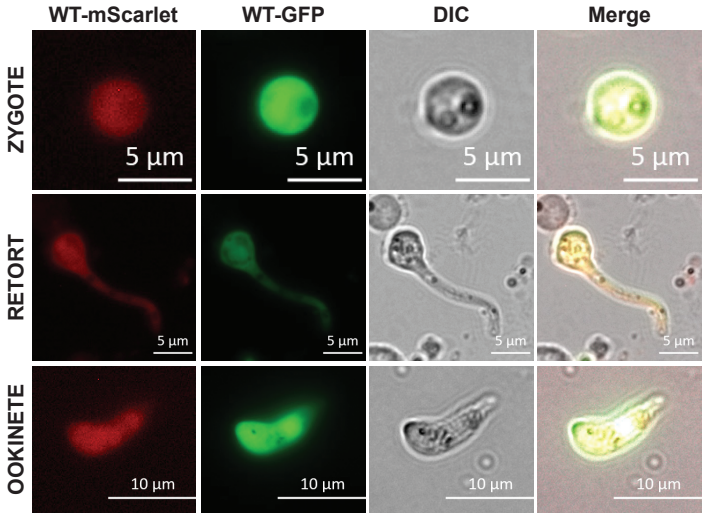

	mScarlet+ Only Retorts/Ookinetes	GFP+ Only Retorts/Ookinetes	GFP+/mScarlet+ Zygotes	GFP+/mScarlet+ Retorts/Ookinetes
WT-mScarlet	35, 90	0, 0	0, 0	0, 0
WT-GFP	0, 0	29, 104	0, 0	0, 00
WT-mScarlet x WT-GFP	11, 15	4, 30	29, 42	23, 39
pynot1-g⁻ Clone 1	0, 0	0, 0	0, 0	0, 0
pynot1-g⁻ Clone 2	0, 0	0, 0	0, 0	0, 0
WT-mScarlet x *pynot1-g*⁻ Clone 1	39, 73	0, 0	49, 24	0, 0
WT-mScarlet x *pynot1-g*⁻ Clone 2	30, 84	0, 0	26, 26	0, 0

Hart *et al.* Figure 5

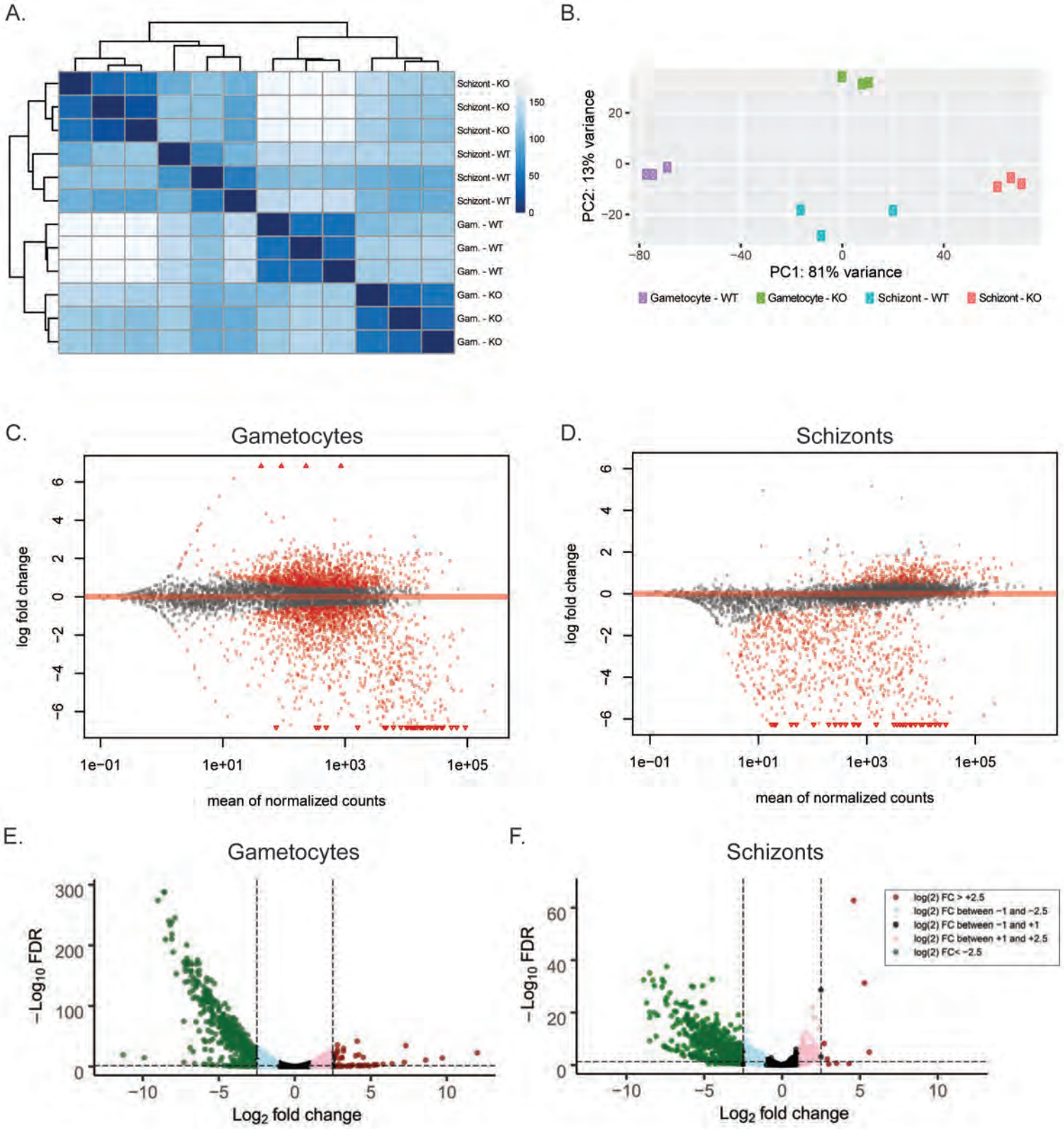

Hart *et al.* Figure 6

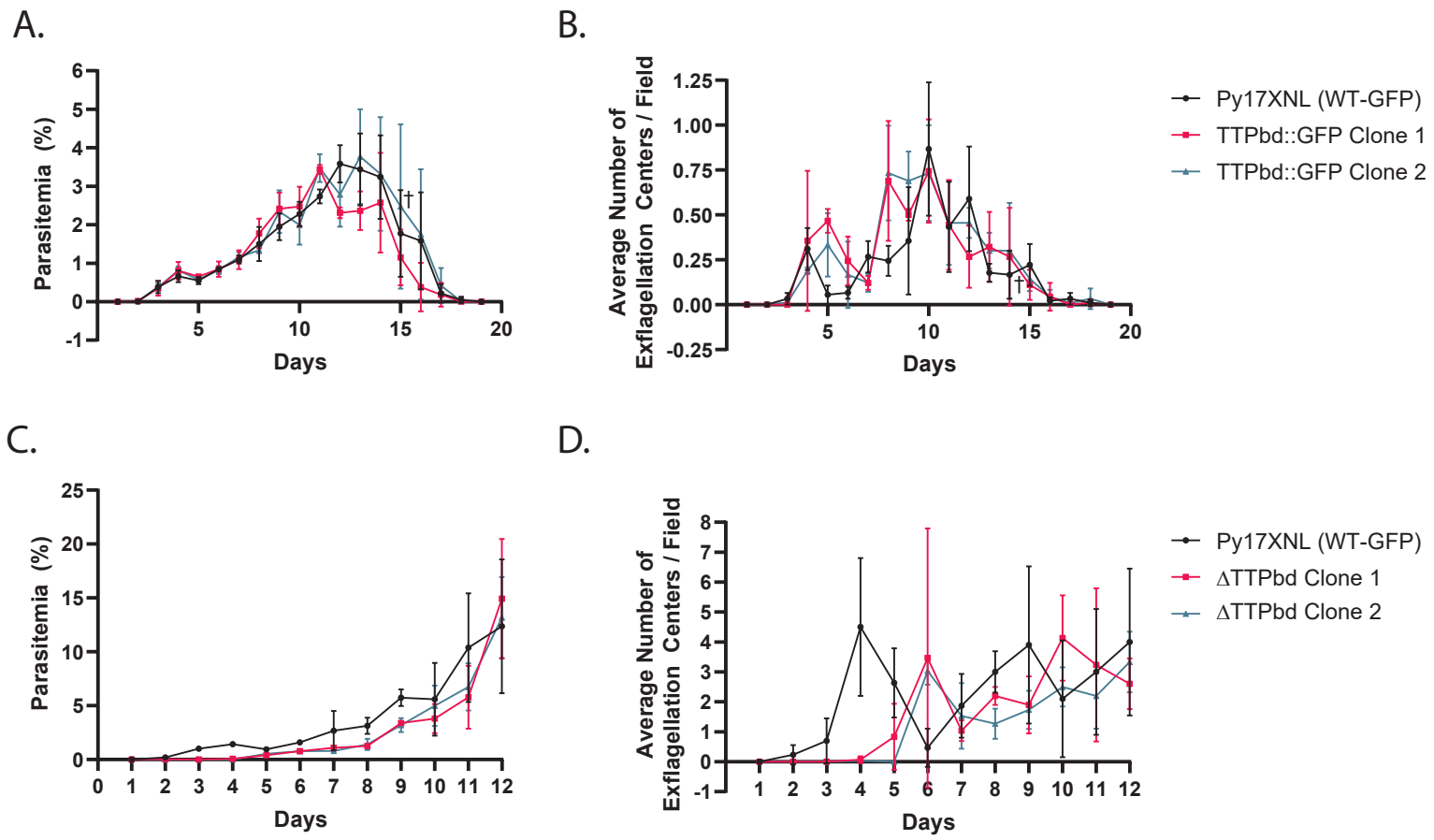

Hart *et al.* Figure 7

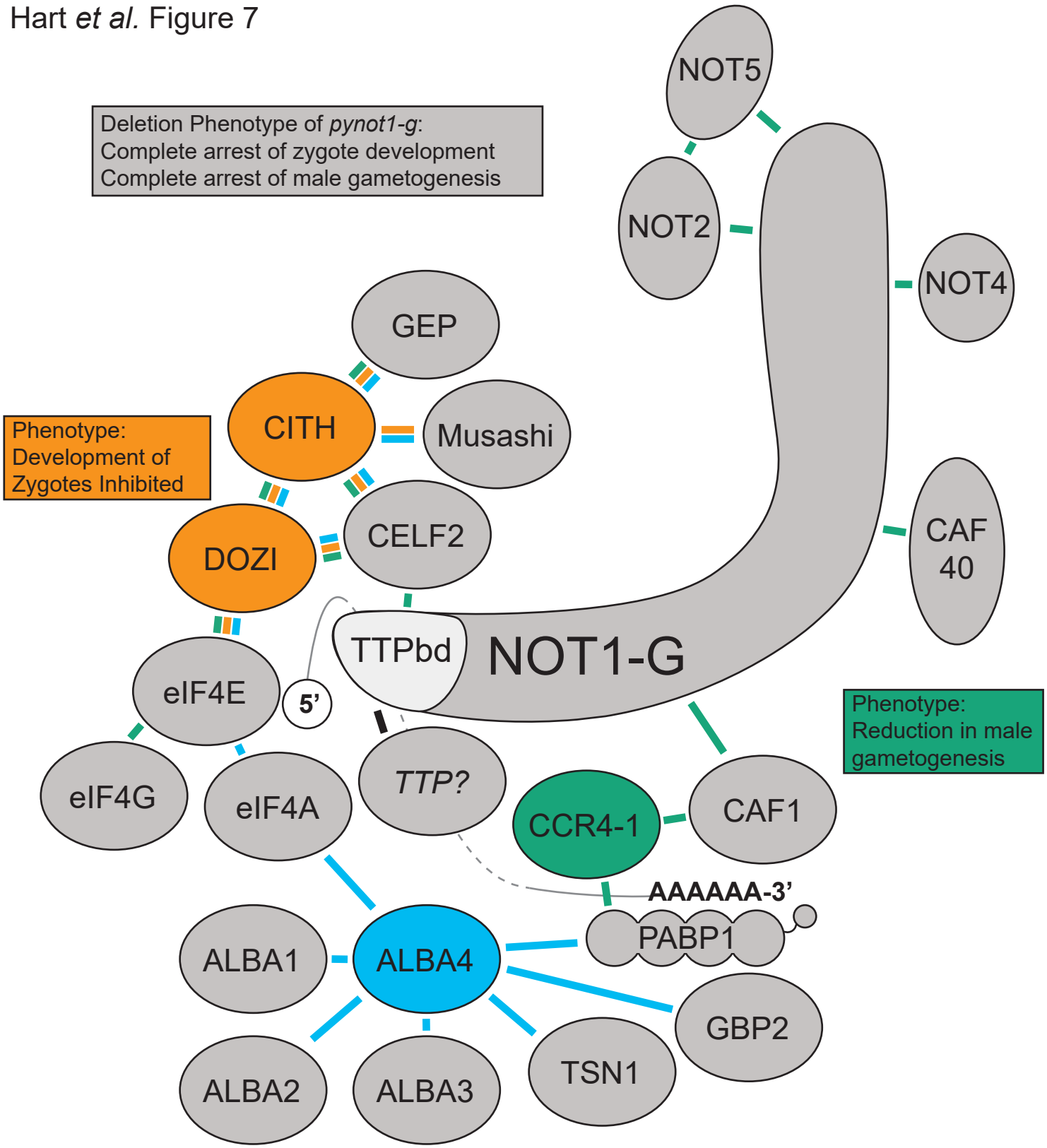

Figure 7: A proposed composite interaction network of NOT1-G. Crosslinking IP datasets for PbDOZI and PbCITH (orange lines), PyCCR4-1 (green lines), and PyALBA4 (light blue lines) were used to propose a composite interaction network with PyNOT1-G. The placement of some proteins is based upon known direct interactions from the literature (e.g. NOT1-G, CAF1, CCR4, CAF40, NOT4, NOT2, NOT5, PABP1, CELF2, DOZI, eIF4F (eIF4E, eIF4A, eIF4G), as are the placements of the 5' m7G cap next to the cap-binding protein eIF4E and the poly(A) tail with PABP1. Deletion phenotypes for *pynot1-g* match or exceed those of *pbdozi-*, *pyccr4-1-*, and the *pycaf1* truncation, and lead to a complete arrest in male gametogenesis and zygote development.